Reviewed Preprint
v1 • November 11, 2024
Not revised

Reviewed Preprint
v2 • October 28, 2026
Revised by authors

Parvalbumin interneuron ErbB4 controls ongoing network oscillations and olfactory behaviours in mice

Bin Hu[1,†], Chi Geng[1,†], Feng Guo[1], Ying Liu[1,2,3], Ran Wang[1], You-Ting Chen[4], Xiao-Yu Hou[2,3]

[1]Research Center for Biochemistry and Molecular Biology, Jiangsu Key Laboratory of Brain Disease Bioinformation, Xuzhou Medical University, Xuzhou, China • [2]State Key Laboratory of Natural Medicines, China Pharmaceutical University, Nanjing, China • [3]School of Life Science and Technology, China Pharmaceutical University, Nanjing, China • [4]Department of Human Anatomy, Xuzhou Medical University, Xuzhou, China

For correspondence: xyhou@cpu.edu.cn

[†] These authors contributed equally to this work.

Competing interests: No competing interests declared

Funding: See page 25

Reviewing editor: Katalin Toth, University of Ottawa, Canada

© 2024, Hu et al. This article is distributed under the terms of the Creative Commons Attribution License, which permits unrestricted use and redistribution provided that the original author and source are credited.

eLife Assessment

This study provides **important** information on the role of ErbB4 expression in parvalbumin-positive cells in relation to olfactory behaviour and circuit dynamics in the olfactory bulb. The central question is both timely and novel, and the findings could shed light on the critical role that ErbB4 may play in modulating olfactory bulb cell function and olfactory perception. The authors conducted a comprehensive set of experiments which provide **solid** evidence in support of their conclusions. However, some concerns remain regarding the technical approaches used, such as spike sorting and control/baseline comparisons.

https://doi.org/10.7554/eLife.101237.2.sa3

Abstract

Parvalbumin (PV)-positive interneurons modulate the processing of odour information. However, little is known about how PV interneurons dynamically remodel neural circuit responses in the olfactory bulb (OB) and their physiological significance. This study showed that a reinforced odour-discrimination task upregulated ErbB4 kinase activity in the mouse OB. ErbB4 knockout in the OB impaired the dishabituation of odour responses and discrimination of complex odours, whereas odour memory or adaptation was not altered in mice. ErbB4-positive neurones were localised throughout the OB, whereas ErbB4 was largely expressed in PV-positive interneurons within the internal and external plexiform layers. Similarly, ErbB4 ablation in PV interneurons disrupted olfactory discrimination and dishabituation in mice. ErbB4 knockout in PV interneurons disrupted the odour-evoked responses of mitral/tufted cells and increased the power of the ongoing local field potential in awake mice. We also observed a decrease in the frequency of miniature inhibitory postsynaptic currents and deficits in stimulus-evoked recurrent and lateral inhibition of mitral cells following PV-ErbB4 loss, suggesting a broad impairment in inhibitory microcircuits. These findings demonstrate that PV-ErbB4 signalling regulates inhibitory microcircuit activity, ongoing oscillations, and OB output, which underlie normal olfactory behaviour.

Introduction

Discriminating chemical cues in the environment is not only necessary for evaluating potential threats, but also influences cognitive and emotional behaviours. The olfactory system dynamically adjusts its sensitivity to odours in response to changes in environmental, motivational, and cognitive states. For example, odour learning improves the performance of olfactory discrimination tests. Habituation and adaptation to successive exposure to an odour lead to decreased behavioural responses, whereas an unexpected odour enhances olfactory salience and

stimulates behavioural dishabituation. Dysfunction in olfactory discrimination has been observed in the early stages of several neurodegenerative disorders and psychiatric diseases (Carnemolla et al., 2020; Walker et al., 2021). Similarly, the olfactory discrimination ability has a significant predictive value for future cognitive decline in healthy ageing individuals (Sohrabi et al., 2012; Uchida et al., 2020; Yoshitake et al., 2022). However, the neural mechanisms underlying the dynamic modulation of olfactory behaviour remain largely unknown.

The olfactory bulb (OB) is the first relay and processing station in the olfactory system. In the OB, odour signals are transformed into informational outputs that are sent to the associated olfactory cortex. As the principal output neurones of the OB, mitral/tufted cells (M/TCs) receive excitatory glutamatergic inputs from olfactory sensory neurones and inhibitory GABAergic inputs from heterogeneous subpopulations of interneurons. An imbalance in the excitation/inhibition onto mitral cells (MCs) impairs olfactory discrimination (Lepousez and Lledo, 2013). Furthermore, overlapping odour-evoked input patterns in the OB undergo reformatting to enhance the discrimination of similar odours, which depends on GABAergic interneurons (Gschwend et al., 2015; Li et al., 2018; Mohamed et al., 2019; Zavitz et al., 2020). GABAergic interneurons in the OB mediate the recurrent and lateral inhibition of MCs. Recurrent inhibition of MCs by granule cells (GCs) increases the frequency of odour-induced activity and facilitates odour discrimination (Aghvami et al., 2022; MacLeod and Laurent, 1996; Nunes and Kuner, 2015). Interglomerular lateral inhibition sharpens or filters the odour-induced output signals of MCs, enhancing the contrast of odour representations and, consequently, the ability to discriminate between similar odours (Egger and Kuner, 2021). Overall, the OB contains various interneuron types that control different olfactory behaviours (Lyons-Warren et al., 2023; Pardasani et al., 2023; Takahashi et al., 2016). Parvalbumin-positive (PV) interneurons form dendrodendritic contacts with neighbouring MCs (Huang et al., 2013; Kato et al., 2013; Matsuno et al., 2017; Miyamichi et al., 2013). Unlike the odour-specific responses of GCs and MCs, PV interneurons exhibit strong responses to a broader range of odours (Kato et al., 2013). M/TCs receive significant inputs from PV interneurons from the external plexiform layer (EPL) (Miyamichi et al., 2013). However, the contribution of PV interneurons to olfactory behaviour and the associated molecular mechanisms are not understood.

GABAergic neurones preferentially express the receptor tyrosine kinase ErbB4 in cortical areas; however, in subcortical regions, ErbB4 is also expressed by non-GABAergic neurones (Bean et al., 2014; Deng et al., 2019; Dominguez et al., 2019; Fazzari et al., 2010; Lin et al., 2018; Mei and Nave, 2014; Shi and Bergson, 2020). ErbB4 kinases are expressed in neuroblasts in the subventricular zone and rostral migratory stream to the OB, implicating ErbB4 signalling in olfactory interneuronal precursor differentiation and olfaction (Anton et al., 2004). ErbB4 regulates the synaptic transmission and plasticity of PV interneurons in the neocortex and hippocampus (Chen et al., 2022; Dominguez et al., 2019; Grieco et al., 2020; Lin et al., 2018). Recently, we found a distinct ErbB4 signalling pathway in PV interneurons of the prefrontal cortex that hinders flexibility in odour-associated memory updating but has no influence on initial olfactory learning and memory (Cai and Shuman, 2022; Xu et al., 2022). However, whether PV neurones express ErbB4 in the OB and whether this affects olfactory behaviour remain unclear.

In this study, we showed that an odour-discrimination task promotes the activation of ErbB4 in the OB. ErbB4-positive neurones are localised throughout the OB, with most being PV-positive interneurons in the internal plexiform layer (IPL) and EPL. In this context, we evaluated the performance of PV-ErbB4 knockout mice in odour discrimination, habituation/dishabituation, and detection threshold tasks. We also explored the effects of ErbB4 in PV interneurons on the odour-evoked activity of MCs and ongoing network oscillations in awake mice, as well as on the inhibitory modulation of MC output. Our findings reveal the physiological significance of PV interneurons via ErbB4 signalling in the dynamic modulation of olfactory behaviour.

Results

Performing an odour discrimination task upregulates the activity of ErbB4 in the OB

First, we examined the levels of ErbB4 protein and its phosphorylated form (p-ErbB4) in mouse OB after a reinforced go/no-go odour discrimination task. A go/go task without odour discrimination was performed as a control (Figure 1A). Adult mice were first trained over 3 days of go/no-go tasks (200 trials per day) to discriminate between a pair of simple odours (water-rewarded isoamyl acetate and unrewarded heptanone) and then to discriminate complex chemical cues (60%/40% binary mixtures of these odours, "6/4" refers to 60% isoamyl acetate + 40% heptanone, and "4/6" refers to 40% isoamyl acetate + 60% heptanone, in volume) (Figure 1B). As shown in Figure 1C and 1D (see Figures 1 and 2 and Supplementary Figure 1A and 1 B for uncropped western blot images), the level of p-ErbB4 in the go/no-go group was higher than that in the go/go group, implying a link between increased ErbB4 activity in the OB and olfactory discrimination ability.

Therefore, we evaluated whether OB ErbB4 affects the performance of mice in the go/no-go task. Bulbar ErbB4 deficiency was induced by the delivery of adeno-associated virus recombinants expressing Cre recombinase and green fluorescent protein (AAV-Cre-GFP) into both sides of the OB of neonatal mice carrying *loxP*-flanked *Erbb4* alleles (Figure 1E-1G, see Figures 1 and 2 and Supplementary Figure 1C for uncropped western blot images). When learning to discriminate simple odour pairs (Figure 1H), both AAV-GFP– and AAV-Cre-GFP-injected mice reached an accuracy of > 90% within 3 days (~600 trials), suggesting that ErbB4 in the OB has no influence on learning, memory, or the sense of smell. However, when distinguishing between similar odours, the AAV-GFP group achieved accuracy above 80% after the 4-day training program (~800 trials), whereas the AAV-Cre-GFP-injected mice showed significantly lower accuracy. This indicates that ErbB4 in the OB maintains the ability of mice to discriminate between complex odours.

We conducted a habituation/dishabituation test to assess the spontaneous behavioural responses of mice to repeatedly presented odours in the absence of any reward (Figure 1I) to further determine the role of the OB ErbB4 in olfactory behaviours. Both AAV-GFP and AAV-Cre-GFP groups were habituated to four successive odour presentations with 2-min intertrial intervals, and their behavioural responses to the same odour (isoamyl acetate) were progressively reduced. AAV-GFP mice rapidly dishabituated, and their investigation time increased when a novel odour was presented (limonene, fifth trial), whereas AAV-Cre-GFP mice did not show significantly altered behavioural responses to the novel odour. Additionally, the olfactory detection thresholds for isoamyl acetate and limonene were approximately 10^{-5} in AAV-GFP mice, but 10^{-4} in AAV-Cre-GFP mice (Figure 1J and 1K). In the habituation and dishabituation tasks, the two odours were used at levels far above the threshold.

These results demonstrate that ErbB4 in the OB contributes to olfactory discrimination and dishabituation but not to olfactory memory and habituation.

ErbB4 is expressed in PV interneurons within the EPL and IPL layers of the OB

RNAscope analysis was performed to detect mRNA levels of *Erbb4* in the OB of PV-*Erbb4*$^{+/+}$ mice. As shown in Figure 2A-2D, *Erbb4* mRNA was present in all five layers of the OB in PV-*Erbb4*$^{+/+}$mice (green); *Erbb4*-expressing neurones accounted for 74.0%, 61.2%, 69.1%, 74.9%, and 84.4% of the total cells (DAPI, blue) in the glomerular layer (GL), EPL, mitral cell layer (MCL), IPL, and granule cell layer (GCL), respectively (Figure 2D). PV interneurons (red) in the OB were primarily localised to the EPL and IPL (Figure 2A), where *Erbb4* mRNA tended to be located within PV interneurons (yellow) (Figure 2A-2C). Of the PV interneurons in the EPL and IPL, 84.6% and 100% expressed *Erbb4*, respectively (Figure 2E). Overall, *Erbb4* mRNA levels in PV interneurons were the highest in the IPL and lowest in the EPL.

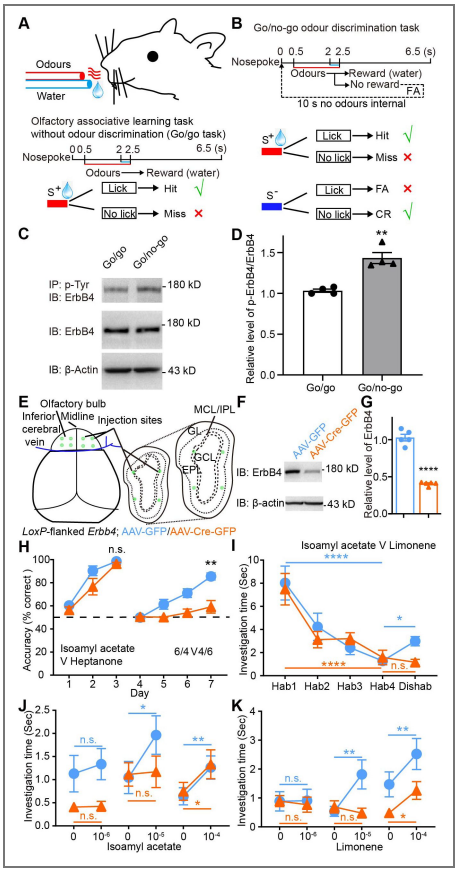


Figure 1. ErbB4 in the OB is critical for odour discrimination and dishabituation.

(A) Behavioural paradigm for olfactory associative learning without odour discrimination (go/go task). Mice inserted their snout into the sampling port to trigger odours. The schematic describes the timeline of a single trial. Mice learned to lick the metal tube to receive water in response to either of the odours in the pair (reward, hit). (B) Timeline for a single trial in the go/no-go odour discrimination task. Mice learned to avoid licking the metal tube for the unrewarded odour (correct rejection, CR). Licking when presented with the unrewarded odour (false alarm, FA) led to no water reward and a timeout of up to 10 s. (C and D) ErbB4 activity in the OB was elevated after training on the reinforced go/no-go odour discrimination task. OB cell lysates were subjected to the IP or IB using the indicated antibodies. Relative p-ErbB4/ErbB4 levels were normalized to their respective control groups in the western blot analysis. (n = 4 mice per group, $t_{(6)}$ = 5.75, P = 0.0012, unpaired t test). (E) Schema indicating virus injection sites. To specifically delete ErbB4 protein in the OB, AAV-Cre-GFP was injected into bilateral OB of neonatal *loxP*-flanked *Erbb4* mice. (F and G) Reduced ErbB4 expression in the OB of a mouse injected with AAV-Cre-GFP (n = 5 mice per group, $t_{(8)}$ = 24.7, P < 0.0001, unpaired t test). (H) Odour discrimination performance under the reinforced go/no-go task. The accuracy for simple odour pairs was similar for the control and experimental groups (n = 8 mice per group, $F_{(1, 14)}$ = 2.83, P = 0.1148, two-way ANOVA). However, the accuracy for difficult odour mixtures (6/4 V 4/6) was reduced in AAV-Cre-GFP mice ($F_{(1, 14)}$ = 16.14, P = 0.0013, two-way ANOVA). (I) Olfactory behavioural performance under a spontaneous habituation/dishabituation task. Both animal groups showed a decline in investigation time to isoamyl acetate over the habituation period (n = 9 AAV-GFP mice, P < 0.0001; n = 10 AAV-Cre-GFP mice, P < 0.0001, $F_{(3, 51)}$ = 21.83, two-way ANOVA). However, AAV-GFP ($F_{(1, 17)}$ = 3.52, P = 0.0065), but not AAV-Cre-GFP mice (P = 0.6296, two-way ANOVA), showed an increase in investigation time toward limonene in the dishabituation period. (J) Odour detection threshold to isoamyl acetate. For AAV-GFP mice, the sniffing time toward isoamyl acetate was significantly higher than that for mineral oil at concentrations of 10^{-5} and 10^{-4}, but not 10^{-6}. (n = 12 mice, $F_{(1, 21)}$ = 0.19, 4.18 and 14.88, P = 0.5689, 0.0111, and 0.0090, two-way ANOVA). These results show that AAV-GFP mice were able to detect isoamyl acetate at a concentration of 10^{-5}. For AAV-Cre-GFP mice, the sniffing time toward isoamyl acetate was significantly higher than that for mineral oil at a concentration of 10^{-4}, but not at concentrations of 10^{-5} and 10^{-6} (n = 11 mice, P = 0.9672, 0.8713, and 0.0172, two-way ANOVA). These results show that AAV-Cre-GFP mice only detect isoamyl acetate at a concentration of 10^{-4}. (K) Similarly, AAV-GFP mice were able to detect limonene at a concentration of 10^{-5} (n = 12 mice, $F_{(1, 21)}$ = 0.03, 4.77 and 12.96, P = 0.9603, 0.0011, and 0.0069, two-way ANOVA), whereas AAV-Cre-GFP mice only detected limonene at a concentration of 10^{-4} (n = 11 mice, P = 0.7671, 0.5490, and 0.0463, two-way ANOVA). Data are presented as means ± s.e.m. * P < 0.05, ** P < 0.01, **** P < 0.0001, n.s. = not significant. EPL, external plexiform layer; GCL, granule cell layer; GL, glomerular layer; IPL, internal plexiform layer; MCL, mitral cell layer.

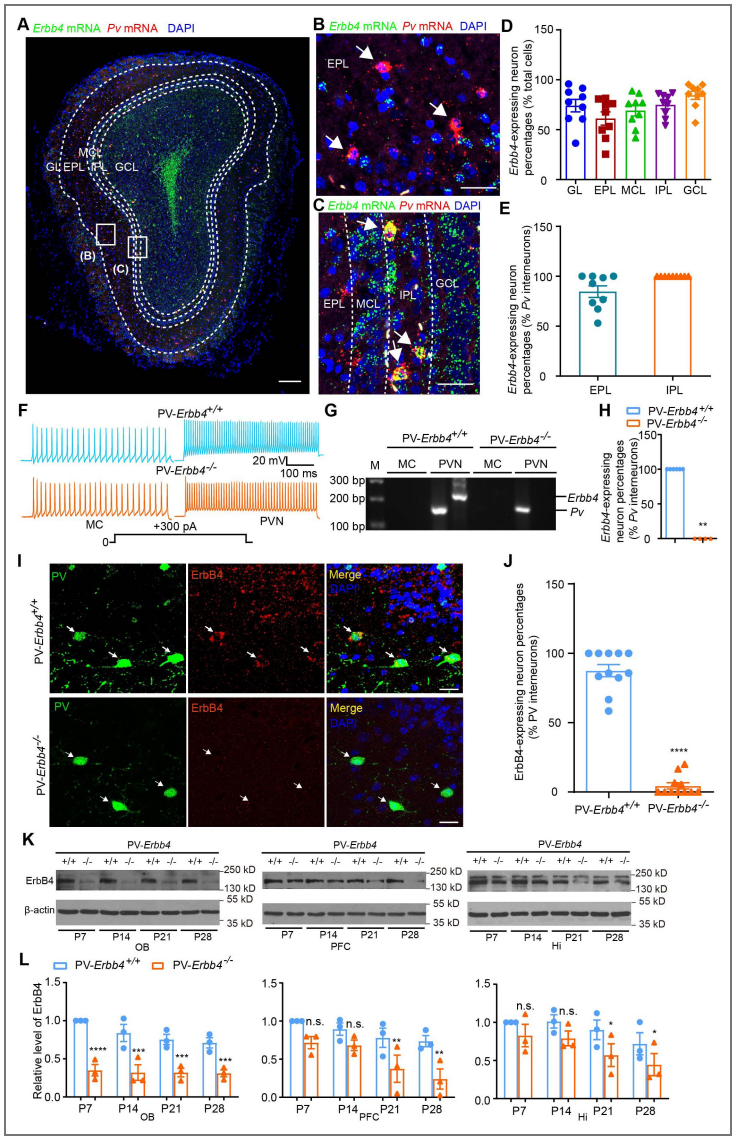


Figure 2. ErbB4 proteins are largely expressed in PV interneurons in the OB.

(A) *In vitro* imaging of ErbB4 mRNA in sections from PV-*Erbb4*$^{+/+}$ mice. Double single-molecule fluorescence in situ hybridization of ErbB4 (green) and PV (red) in the OB. Scale bar, 200 μm. (B) Magnified view of the EPL box from A. Scale bar, 50 μm. (C) Magnified view of the IPL box from A. Scale bar, 50 μm. (D) Summarized data showing the proportion of ErbB4-expressing neurons in different layers (n = 9 slices from 4 mice). (E) Summarized data showing the proportion of the ErbB4/PV double-positive neurons relative to the total number of PV interneurons in the EPL and IPL (*n* = 9 slices from 4 mice). DAPI staining was used to determine the total number of cells. (F) *In vitro* electrophysiology experiments performed in slices from PV-*Erbb4*$^{+/+}$ or PV-*Erbb4*$^{-/-}$ mice. Representative examples of action potentials (APs) elicited by positive current injection (500 ms, 300 pA), recorded from an MC (left) and a fast-spiking PV interneuron (right). (G and H) Corresponding single-cell RT-PCR analyses showing that ErbB4 mRNA is detected only in PV interneurons (PVN) from PV-*Erbb4*$^{+/+}$ OB (*n* = 6 and 4 neurons from 4 mice, *P* = 0.0048, unpaired *t* test). DI1000 was used as the size reference (M, 300, 200 and 100 base-pair fragments are indicated). (I and J) Specific deletion of ErbB4 in EPL PV interneurons of the OB (*n* = 11 slices from 4 mice per group, $t_{(20)}$ = 16.91, *P* < 0.0001, unpaired *t* test). OB sections from PV-*Erbb4*$^{+/+}$ and PV-*Erbb4*$^{-/-}$ mice (P28) were stained with anti-PV, ErbB4 and DAPI antibody. Scale bars represent 20 μm. (K and L) Western blots showing that ErbB4 in PV-*Erbb4*$^{-/-}$ OB was largely reduced from P7 onward, whereas ErbB4 in the PFC and hippocampus began to decrease only at P21. Relative levels were normalized to their respective P7 groups of control littermates (*n* = 3 mice per group, OB: $F_{(1, 8)}$ = 245.70, *P* < 0.0001, *P* = 0.0002, 0.0006, and 0.0010; PFC: $F_{(1, 8)}$ = 61.20, *P* = 0.0532, 0.1791, 0.0075, and 0.0021; Hi: $F_{(1, 8)}$ = 38.25, *P* = 0.2585, 0.1005, 0.0139 and 0.0382, two-way ANOVA). Data are presented as means ± s.e.m. * *P* < 0.05, ** *P* < 0.01, *** *P* < 0.001, **** *P* < 0.001, n.s. = not significant. EPL, external plexiform layer; GCL, granule cell layer; GL, glomerular layer; Hi, hippocampus; MCL, mitral cell layer; PFC, prefrontal cortex.

To further ascertain *Erbb4* mRNA expression of individual PV interneurons within EPL and IPL, we conducted patch-clamp electrophysiology followed by single-cell analysis of reverse transcription-polymerase chain reaction (RT-PCR) in OB slices from PV-*Erbb4*$^{+/+}$and PV-ErbB4 conditional knockout (PV-*Erbb4*$^{-/-}$) mice. In addition to their morphology, size, and location, MCs were electrophysiologically characterised as having low-frequency spike discharges (<100 Hz). In contrast, PV interneurons were identified based on their high-frequency spike discharges (>100 Hz) (Figure 2F). The cytosolic contents from identified MCs and PV neurones were then subjected to RT-PCR, showing that *Erbb4* mRNA was only present in PV interneurons from PV-*Erbb4*$^{+/+}$OB, but not in any of the MCs or PV interneurons from PV-*Erbb4*$^{-/-}$OB (Figure 2G and 2H).

Immunofluorescence analysis showed that ErbB4 immunoreactivity within the EPL was present in PV interneurons of PV-*Erbb4*$^{+/+}$ mice; this was largely diminished in PV-*Erbb4*$^{-/-}$ mice (Figure 2I and J). Western blots showed that the levels of ErbB4 proteins were largely reduced, but not abolished, in the OB, prefrontal cortex (PFC), and hippocampus (Hi) of PV-*Erbb4*$^{-/-}$ mice compared with their control littermates (Figure 2K and 2L, see Figures 1 and 2 and Supplementary Figure 1D for uncropped western blot images). This suggests that ErbB4 is largely expressed in the OB PV interneurons. Interestingly, ErbB4 deletion in the OB occurred at least 2 weeks prior to deletion in the prefrontal cortex and hippocampus (Figure 2K and 2L). Nissl staining showed that the overall lamina structures of the OB were not affected in PV-*Erbb4*$^{-/-}$ mice (Figure 2 and Supplementary Figure 2).

These results demonstrate the strong expression of ErbB4 in PV fast-spiking interneurons within the EPL and IPL layers of the OB.

ErbB4 in PV interneurons is necessary for olfactory behaviours

To determine the contribution of ErbB4 expressed in PV interneurons to olfactory behaviours, we conducted reinforced go/no-go tests of olfactory discrimination in PV-*Erbb4*$^{+/+}$and PV-*Erbb4*$^{-/-}$ mice. Both groups learned to distinguish distinct odour pairs with more than 90% accuracy within 600 trials (Figure 3A); PV-*Erbb4*$^{-/-}$mice exhibited significantly lower accuracy than their control littermates for similar odour pairs (Figure 3A). During habituation/dishabituation tasks, both groups of mice habituated to the successive presentation of a familiar odour (isoamyl acetate, fourth trial) (Figure 3B); when a novel odour (limonene, fifth trial) was presented, PV-*Erbb4*$^{-/-}$ mice did not increase their investigation time, unlike their control littermates (Figure 3B). Similarly, when the order of odour presentation was reversed, the PV-*Erbb4*$^{-/-}$ group showed impaired dishabituation, whereas the PV-*Erbb4*$^{+/+}$ group did not (Figure 3C). The olfactory detection thresholds for isoamyl acetate and limonene were slightly higher in PV-*Erbb4*$^{-/-}$ mice than in PV-*Erbb4*$^{+/+}$ mice (Figure 3D and 3E).

We also tested mice using the buried food test, which depends on the animal's natural tendency to utilise olfactory cues for foraging, to confirm whether the mice could smell volatile odours. As shown in Figure 3F, both PV-*Erbb4*$^{+/+}$ and PV-*Erbb4*$^{-/-}$ mice found the buried pellets rapidly over three consecutive testing days. On trial day 4, the pellet was easily located within a similar timeframe as when the food pellet was made visible by placing it on the surface. This suggested that ErbB4 in PV interneurons is not required for the ability of mice to detect and locate odorous sources.

These findings reveal that ErbB4 signalling in PV interneurons serves as an essential regulator of olfactory discrimination and dishabituation.

ErbB4 in PV interneurons mediates odour-evoked responses of M/TCs in the OB

To investigate the overall functional relevance of ErbB4 signalling in PV interneurons in regulating M/TC responses, we recorded extracellular spontaneous and odour-evoked activity from M/TCs in the OB via tetrodes implanted in awake, head-fixed PV-*Erbb4*$^{-/-}$ and PV-*Erbb4*$^{+/+}$ mice (Figure 4A). To obtain individual neuronal spikes, units were identified using principal component

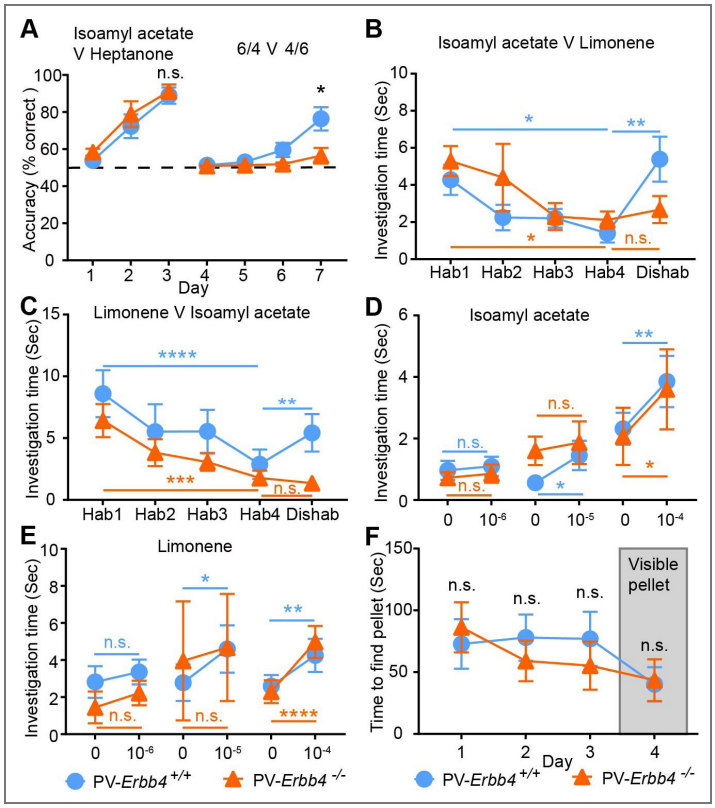


Figure 3. ErbB4 in PV interneurons is critical for olfactory behaviours.

(A) Odour discrimination under the reinforced go/no-go task in PV-*Erbb4*$^{-/-}$ mice. The accuracy for simple odour pairs was indistinguishable (n = 5 and 6 mice, $F_{(1, 9)}$ = 0.70, P = 0.4260, two-way ANOVA). However, the accuracy for difficult odour pairs was significantly lower in PV-*Erbb4*$^{-/-}$mice ($F_{(1, 9)}$ = 9.12, P = 0.0144, two-way ANOVA). (B) Olfactory behavioural performance under the spontaneous habituation/dishabituation task. Both animal groups habituated to isoamyl acetate (n = 12 mice per group, $F_{(3, 66)}$ = 6.68, P = 0.0349 and 0.0164, two-way ANOVA). However, PV-*Erbb4*$^{+/+}$mice ($F_{(1, 22)}$ = 8.93, P = 0.0025), but not PV-*Erbb4*$^{-/-}$mice (P = 0.8451, two-way ANOVA), dishabituated to limonene. (C) Olfactory behavioral performance under the reversed habituation/dishabituation task. Both animal groups habituated to limonene ($F_{(3, 54)}$ = 16.33, P < 0.0001 and 0.0003, two-way ANOVA). However, PV-*Erbb4*$^{+/+}$ mice ($F_{(1, 18)}$ = 5.22, P = 0.0023), but not PV-*Erbb4*$^{-/-}$mice (P = 0.7890, two-way ANOVA), dishabituated to isoamyl acetate. (D) PV-*Erbb4*$^{+/+}$mice were able to detect isoamyl acetate at a concentration of 10^{-5} (n = 10 mice, $F_{(1, 18)}$ = 0.60, 3.74 and 16.69, P = 0.6069, 0.0498, and 0.0096 for 10^{-6}, 10^{-5}, and 10^{-4}, two-way ANOVA). PV-*Erbb4*$^{-/-}$ mice only detected isoamyl acetate at a concentration of 10^{-4} (n = 10 mice, P = 0.5764, 0.5353, and 0.0100 for 10^{-6}, 10^{-5}, and 10^{-4}, two-way ANOVA). (E) PV-*Erbb4*$^{+/+}$ mice could detect limonene at a concentration of 10^{-5} (n = 10 mice, $F_{(1, 18)}$ = 1.75, 7.95 and 32.51, P = 0.4540, 0.0106, and 0.0064 for 10^{-6}, 10^{-5}, and 10^{-4}, two-way ANOVA). PV-*Erbb4*$^{-/-}$ mice only detected limonene at a concentration of 10^{-4} (n = 10 mice, P = 0.2842, 0.2709, and < 0.0001 for 10^{-6}, 10^{-5}, and 10^{-4}, two-way ANOVA). (F) The latency for mice to locate the buried and visible food pellets did not differ between the groups (n = 14 and 11 mice, for the buried food pellet, $F_{(1, 23)}$ = 0.21, P = 0.9786, 0.9279, and 0.8873; for the visible food pellet, P > 0.9999, two-way ANOVA). Data are presented as means ± s.e.m. * P < 0.05, ** P < 0.01, *** P < 0.001, **** P < 0.0001, n.s. = not significant.

analysis (PCA) scan clustering of the spikes (Figure 4 and Supplemental Figure 1A and 1B). ErbB4 deletion in PV interneurons did not directly affect the spike waveform of M/TCs *in vivo*, with no significant differences in peak-to-valley ratio or half-valley width between PV-*Erbb4*$^{-/-}$ and PV-*Erbb4*$^{+/+}$mice (Figure 4, Supplementary Figure 1C–1E). Both excitatory (upper, odour-evoked firing rate > spontaneous firing rate) and inhibitory (lower, odour-evoked firing rate < spontaneous firing rate) responses were observed upon odour presentation using the odour delivery system (Figure 4B and 4C). Figure 4D shows the heat maps of odour-evoked changes in mean firing rate (ΔMFR) of 240 M/TCs in PV-*Erbb4*$^{+/+}$ mice (left) and 232 M/TCs in PV-*Erbb4*$^{-/-}$ mice (right). As shown in Figure 4E, spontaneous firing of M/TCs was similar in PV-*Erbb4*$^{+/+}$ and PV-*Erbb4*$^{-/-}$ groups; odour-evoked firing of M/TCs was reduced by ErbB4 deletion in PV interneurons. Both the absolute value of odour-evoked changes in mean firing rate (ΔMFR) and the signal-to-noise ratio (SNR) were lower in PV-*Erbb4*$^{-/-}$ M/TCs than in PV-*Erbb4*$^{+/+}$ M/TCs (Figure 4E).

We next analysed the differences in M/TCs with excitatory responses (Figure 4F and 4G), inhibitory responses (Figure 4H and 4I), and no responses (Figure 4J and 4K) to odour presentation in PV-*Erbb4*$^{+/+}$ and PV-*Erbb4*$^{-/-}$ mice. Compared with the PV-*Erbb4*$^{+/+}$ group, PV-*Erbb4*$^{-/-}$ M/TCs had significantly higher spontaneous firing rates for excitatory responses (Figure 4G). The odour-evoked firing rate was not changed by ErbB4 deletion in PV interneurons. The odour-evoked changes in ΔMFR and SNR markedly decreased in PV-*Erbb4*$^{-/-}$ M/TCs (Figure 4F and 4G). Compared with the PV-*Erbb4*$^{+/+}$group, M/TCs in PV-*Erbb4*$^{-/-}$ mice exhibited significantly lower spontaneous and odour-evoked inhibitory firing rates (Figure 4I). Interestingly, the odour-evoked changes in ΔMFR and SNR also showed a slight decrement in PV-*Erbb4*$^{-/-}$ M/TCs (Figure 4H and 4I). Spontaneous and odour-evoked firing rates for M/TCs classes that had no responses during odour presentation were higher in PV-*Erbb4*$^{-/-}$ group than in the PV-*Erbb4*$^{+/+}$ group (Figure 4K). The absolute values of odour-evoked changes (ΔMFR) and SNR showed no differences between the two groups (Figure 4J and 4K). Furthermore, the distribution of types of odour-evoked responses was significantly altered in PV-*Erbb4*$^{-/-}$ mice compared with PV-*Erbb4*$^{+/+}$ mice (Figure 4L), suggesting compromised odour detection.

These results demonstrate that ErbB4 signalling in PV interneurons mediates the fine-tuning of M/TC odour-evoked responses.

ErbB4 in PV interneurons decreases the power of the ongoing oscillations

Next, we investigated the overall functional relevance of ErbB4 in PV interneurons by examining whether their deletion affects spontaneous oscillations in the OB. Raw local field potential (LFP) signals were divided into different frequency bands: theta (2–12 Hz), beta (15–35 Hz), low gamma (36–65 Hz), and high gamma (66–95 Hz) (Figure 5A). For all frequency bands of the ongoing baseline LFP, the power was higher in PV-*Erbb4*$^{-/-}$ mice than in PV-*Erbb4*$^{+/+}$ mice (Figure 5B-5I), suggesting that ErbB4 signalling in PV interneurons controls the spontaneous ongoing network oscillations in the OB.

ErbB4 in PV interneurons regulates the OB output

To further evaluate the physiological role of the PV interneuron ErbB4 in the regulation of OB output, we recorded the spontaneous and evoked excitatory firing rates from the principal MCs (output cells) in OB slices. Cell-attached recordings showed that the frequency of MC spontaneous action potentials (sAPs) was dramatically enhanced in PV-*Erbb4*$^{-/-}$ mice compared with PV-*Erbb4*$^{+/+}$ mice (Figure 6A and 6B). Furthermore, the frequency of evoked action potentials (eAPs) was also higher in PV-*Erbb4*$^{-/-}$ mice (Figure 6A and 6B). However, the ratio of eAP to sAP firing (i.e., the SNR) was significantly lower in PV-*Erbb4*$^{-/-}$ mice (Figure 6A and 6B). More importantly, the SNR in response to stimuli at various intensities was lower in PV-*Erbb4*$^{-/-}$ mice than in their control littermates (Figure 6C and 6D), even though the overall current-evoked activity was elevated in PV-*Erbb4*$^{-/-}$ mice compared with their control littermates (Figure 6E and 6F).

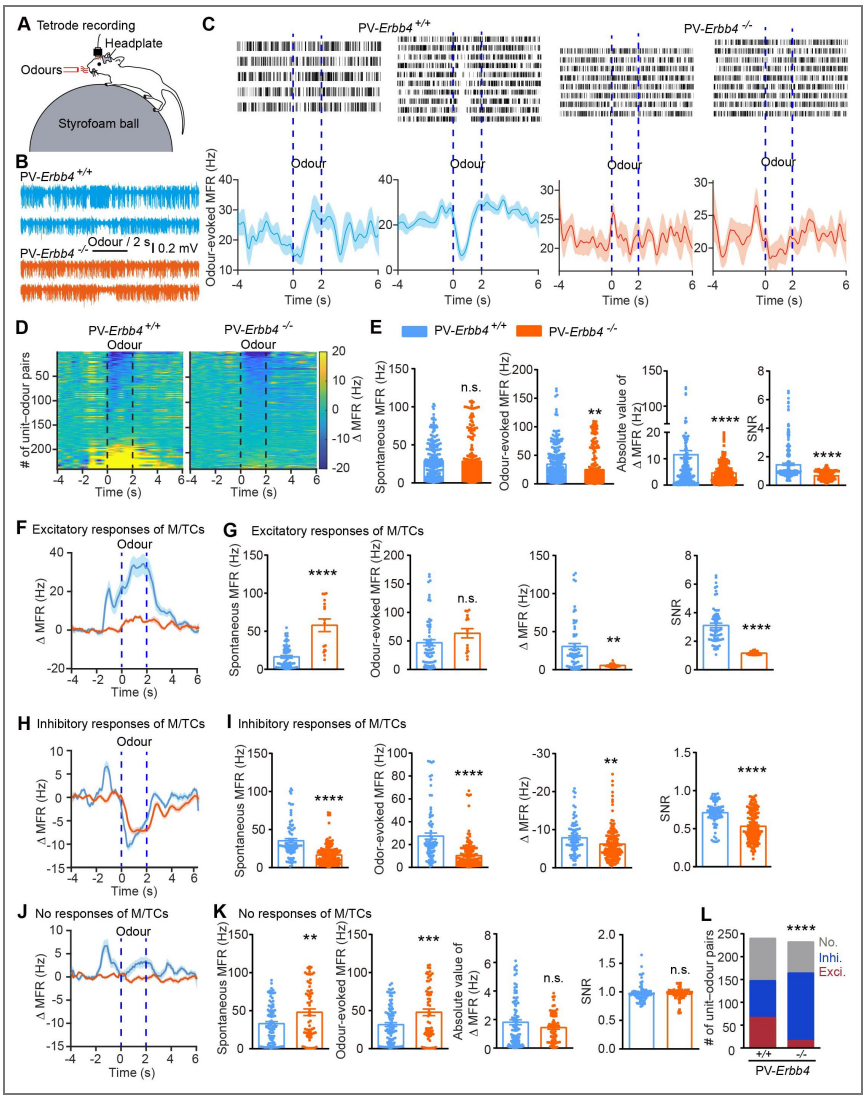


Figure 4. Odour-evoked responses in M/TCs are decreased in PV-*Erbb4*$^{-/-}$ mice.

(A) Schematic of *in vivo* odour-evoked electrophysiological recordings in awake, head-fixed mice with ErbB4 knocked out in PV interneurons. (B) Representative raw traces of spike activity before (spontaneous), during (odour-evoked), and after 2-s odour stimulation in PV-*Erbb4*$^{+/+}$ and PV-*Erbb4*$^{-/-}$ mice. (C) Examples of raster plots (top) and PSTHs of the firing rate (bottom) for odour-evoked excitatory (left) and inhibitory (right) responses in PV-*Erbb4*$^{+/+}$and PV-*Erbb4*$^{-/-}$ mice. PSTHs were smoothed with a Gaussian filter with a standard deviation of 1500 ms. (D) Heat maps of the odour-evoked changes in mean firing rate (ΔMFR) across all unit–odour pairs in PV-*Erbb4*$^{+/+}$mice (n = 240 unit–odour pairs from 4 mice) and PV-*Erbb4*$^{-/-}$mice (n = 232 unit–odour pairs from 4 mice). (E) Quantitative analysis of the spontaneous firing rate ($t_{(470)}$ = 0.27, P = 0.7899), odour-evoked MFR ($t_{(470)}$ = 3.30, P = 0.0010), absolute value of odour-evoked changes ($t_{(470)}$ = 5.05, P < 0.0001), and SNR ($t_{(470)}$ = 9.29, P < 0.0001, unpaired t test) across all unit–odour pairs. (F) Odour-evoked excitatory changes in MFR (ΔMFR) for M/TCs recorded from PV-*Erbb4*$^{+/+}$ mice (n = 66 unit–odour pairs from 4 mice) and PV-*Erbb4*$^{-/-}$ mice (n = 16 unit–odour pairs from 4 mice). (G) Quantitative analysis of the spontaneous firing rate ($t_{(80)}$ = 7.67, P < 0.0001), odour-evoked MFR ($t_{(80)}$ = 1.43, P = 0.1578), odour-evoked ΔMFR ($t_{(80)}$ = 3.10, P = 0.0027), and SNR ($t_{(80)}$ = 5.91, P < 0.0001, unpaired t test) across excitatory unit–odour pairs. (H) Odour-evoked inhibitory ΔMFR for M/TCs recorded from PV-*Erbb4*$^{+/+}$mice (n = 81 unit–odour pairs from 4 mice) and PV-*Erbb4*$^{-/-}$mice (n = 148 unit–odour pairs from 4 mice). (I) Quantitative analysis of spontaneous firing rate ($t_{(227)}$ = 7.52, P < 0.0001), odour-evoked MFR ($t_{(227)}$ = 7.23, P < 0.0001), odour-evoked ΔMFR ($t_{(227)}$ = 2.72, P = 0.0070), and SNR ($t_{(227)}$ = 6.91, P < 0.0001, unpaired t test) across inhibitory unit–odour pairs. (J) ΔMFR for units with no response to odour in PV-*Erbb4*$^{+/+}$ mice (n = 93 unit–odour pairs from 4 mice) and PV-*Erbb4*$^{-/-}$ mice (n = 68 unit–odour pairs from 4 mice). (K) Quantitative analysis of spontaneous firing rate ($t_{(159)}$ = 3.13, P = 0.0021), odour-evoked MFR ($t_{(159)}$ = 3.38, P = 0.0009), absolute value of ΔMFR ($t_{(159)}$ = 1.63, P = 0.1057), and SNR ($t_{(159)}$ = 0.43, P = 0.6687, unpaired t test) across "no response" unit–odour pairs. (L) Distribution of excitatory, inhibitory, and "no response" units in PV-*Erbb4*$^{+/+}$ and PV-*Erbb4*$^{-/-}$ mice ($\chi^2_{(2)}$ =53.85, P < 0.0001, Chi-Square tests). ** P < 0.01, *** P < 0.001, **** P < 0.0001, n.s. = not significant.

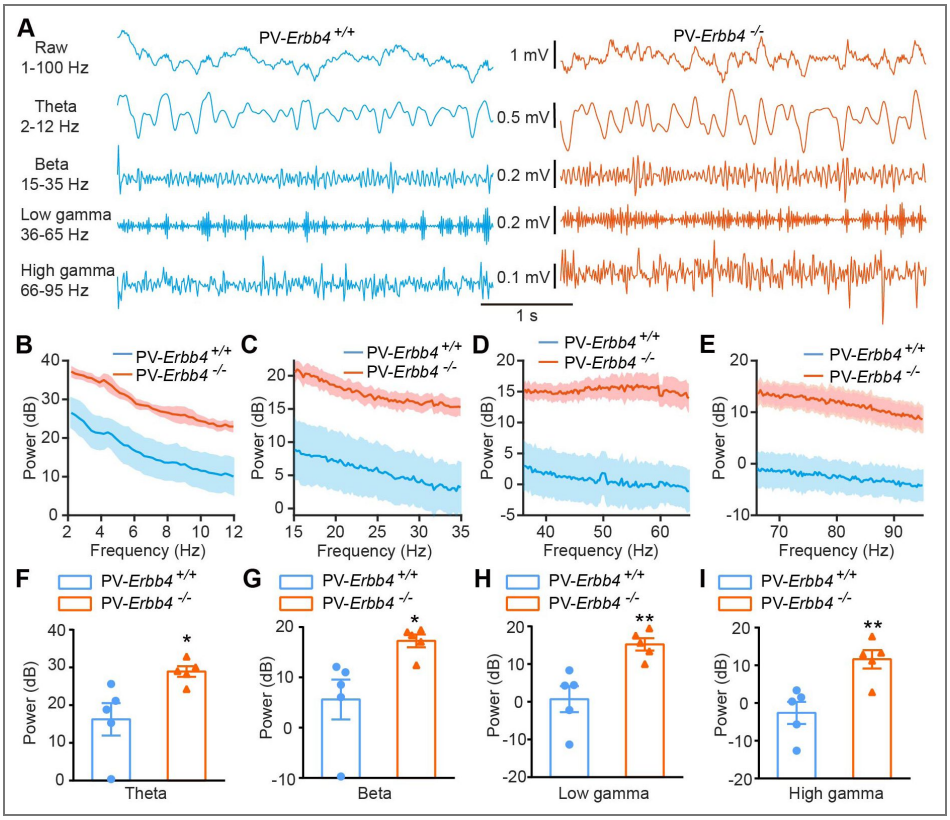


Figure 5. The ongoing LFP in the OB is increased in PV-*Erbb4*$^{-/-}$ mice.

(A) Examples of ongoing LFP signals recorded in the OB from PV-*Erbb4*$^{+/+}$and PV-*Erbb4*$^{-/-}$ mice. The five rows show the raw traces and the filtered theta, beta, low-gamma, and high-gamma signals. (B-E) Quantitative analysis of the averaged power spectra in the theta, beta, low-gamma, and high-gamma bands for the two groups. (F-I) Comparisons of power in the theta (n = 5 mice per group, $t_{(8)}$ = 2.80, P = 0.0233, unpaired t test), beta ($t_{(8)}$ = 2.80, P = 0.0232, unpaired t test), low-gamma ($t_{(8)}$ = 3.80, P = 0.0053, unpaired t test), and high-gamma ($t_{(8)}$ = 3.73, P = 0.0058, unpaired t test) oscillations in the OB in the two groups. * P < 0.05, ** P < 0.01.

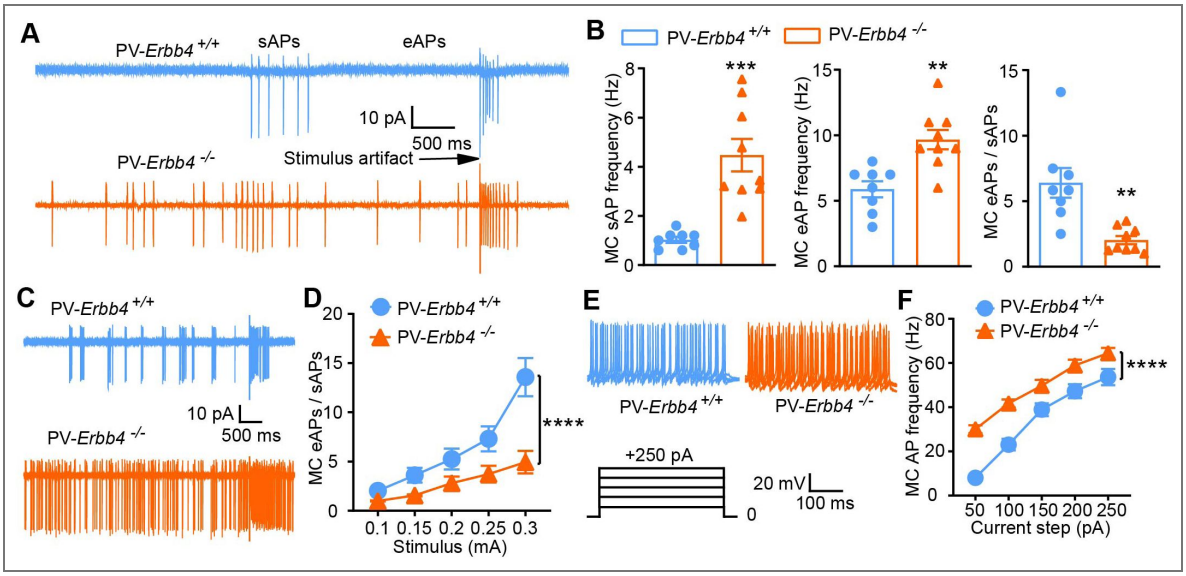


Figure 6. PV-*Erbb4*$^{-/-}$ mice have impaired information output from the OB.

(A and B) Increased frequency of MC sAPs and olfactory nerve-evoked APs (eAPs) in PV-*Erbb4*$^{-/-}$ mice, but decreased ratio of eAPs to sAPs (*n* = 8-9 from 3 mice per group, sAPs: $t_{(15)}$ = 4.84, *P* = 0.0002, eAPs: $t_{(15)}$ = 3.87, *P* = 0.0015; ratio: $t_{(15)}$ = 3.90, *P* = 0.0014, unpaired *t* test). (C and D) The eAP-to-sAP ratio was reduced in PV-*Erbb4*$^{-/-}$ mice as the intensity of the stimulus increased (*n* = 8 from 3 mice per group, $F_{(1, 70)}$ = 32.39, *P* < 0.0001, two-way ANOVA). (E and F) AP frequency elicited by injection of positive currents was higher in PV-*Erbb4*$^{-/-}$ mice than PV-*Erbb4*$^{+/+}$ mice (*n* = 9 from 4 and 3 mice per group, $F_{(1, 80)}$ = 78.9, *P* < 0.0001, two-way ANOVA). Data are presented as means ± s.e.m. ** *P* < 0.01, *** *P* < 0.001, **** *P* < 0.0001.

These data indicate an involvement of PV interneuron ErbB4 in OB odour information processing.

ErbB4 in PV interneurons maintains inhibitory circuit activity in the OB

To investigate the neural mechanisms underlying the observed hyperexcitability in PV-*Erbb4*$^{-/-}$ mouse MCs, we tested whether the effect of ErbB4 deletion in PV interneurons could be occluded by GABAergic blockage. Bicuculline (10 μM), a selective $GABA_A$ receptor antagonist, elevated sAP firing in MCs from PV-*Erbb4*$^{+/+}$ mice but did not further increase MC hyperexcitability in PV-*Erbb4*$^{-/-}$ mice (Figure 7A and 7B). Bicuculline also reduced the eAP:sAP ratio in PV-*Erbb4*$^{+/+}$ MCs but not in PV-*Erbb4*$^{-/-}$MCs (Figure 7A and 7B), suggesting that the impaired output of PV-*Erbb4*$^{-/-}$ MCs depends on GABAergic downregulation. Therefore, we recorded $GABA_A$ receptor-mediated miniature inhibitory postsynaptic currents (mIPSCs) from MCs in whole-cell mode. As shown in Figure 7C and 7D, the mIPSC frequency, but not the amplitude, was significantly reduced in PV-*Erbb4*$^{-/-}$ MCs, suggesting a presynaptic impairment of inhibitory transmission. Neither the frequency nor the amplitude of glutamatergic receptor-mediated miniature excitatory postsynaptic currents (mEPSCs) was altered in PV-*Erbb4*$^{-/-}$MCs compared with their control littermates (Figure 7E and 7F). In contrast, both the frequency and amplitude of mEPSCs in OB PV interneurons were markedly reduced in PV-*Erbb4*$^{-/-}$ mice (Figure 7, Supplementary Figure 1A and 1B). Further analyses of PV interneuron intrinsic properties showed increased action potential frequency in PV-*Erbb4*$^{-/-}$ mice. In contrast, action potential amplitude and half-width remained unaltered (Figure 7, Supplementary Figure 1C-1E), indicating preserved spike waveform following ErbB4 deletion. These results suggest that ErbB4 signalling in PV interneurons regulates olfactory information output by maintaining GABAergic inputs to MCs in the OB.

Next, we examined the effect of a specific PV-ErbB4 knockout on the recurrent inhibition of MCs. Prolonged hyperpolarisation after AP firing, which resulted from recurrent inhibition, was observed in the whole-cell patch-clamp configuration. Although the strength of recurrent inhibition is reported to depend on MC firing rates (Margrie et al., 2001), neither the amplitude nor the decay times of recurrent inhibitory postsynaptic potentials (IPSPs) showed significant alteration with the increment in AP frequency in PV-*Erbb4*$^{-/-}$ mice (Figure 8A and 8B). One possible explanation is that the loss of ErbB4 in the PV interneurons severely impedes recurrent IPSPs. To test this hypothesis, we recorded recurrent IPSPs after a given frequency of APs in PV-*Erbb4*$^{-/-}$ mice. As shown in Figure 8C and Figure 8 and Supplementary Figure 1A, a current injection of 80 pA in PV-*Erbb4*$^{-/-}$ mice elicited approximately the same firing rate as a current injection of 100 pA in PV-*Erbb4*$^{+/+}$ mice. Remarkably, both the amplitude and the decay time constant of the subsequent recurrent IPSP were reduced in PV-*Erbb4*$^{-/-}$mice (Figure 8D). Thus, ErbB4-expressing PV interneurons mediate recurrent inhibition induced by the same MC firing intensity.

In addition, we attempted to isolate broader lateral inhibition between MCs and detect the effects of ErbB4 ablation on it. The recorded MC corresponding to the target glomerulus was visually identified using Alexa 488 dye in a whole-cell patch pipette, as described previously (Hu et al., 2017). A stimulating electrode was then placed into the glomerulus located 3–4 glomeruli (~400 μm) caudally from the target glomerulus. Before recording, we sectioned the GL and the GCL between the sites of conditioning stimulation and the target glomerulus to eliminate interglomerular and GC-mediated lateral inhibition (Figure 8E). As shown in Figure 8F and 8G, a burst of conditioning stimuli (40 pulses at 100 Hz) caused a reduction in the MC firing rate in PV-*Erbb4*$^{+/+}$ mice, but not in PV-*Erbb4*$^{-/-}$ mice. When we cut through the EPL, this broader lateral inhibition was completely abolished in PV-*Erbb4*$^{+/+}$ mice (Figure 8H-8J), indicating that ErbB4-expressing PV interneurons mediate the broader lateral inhibition.

The above data reveal an important contribution of the PV interneuron ErbB4 to the inhibitory circuit activity in the OB.

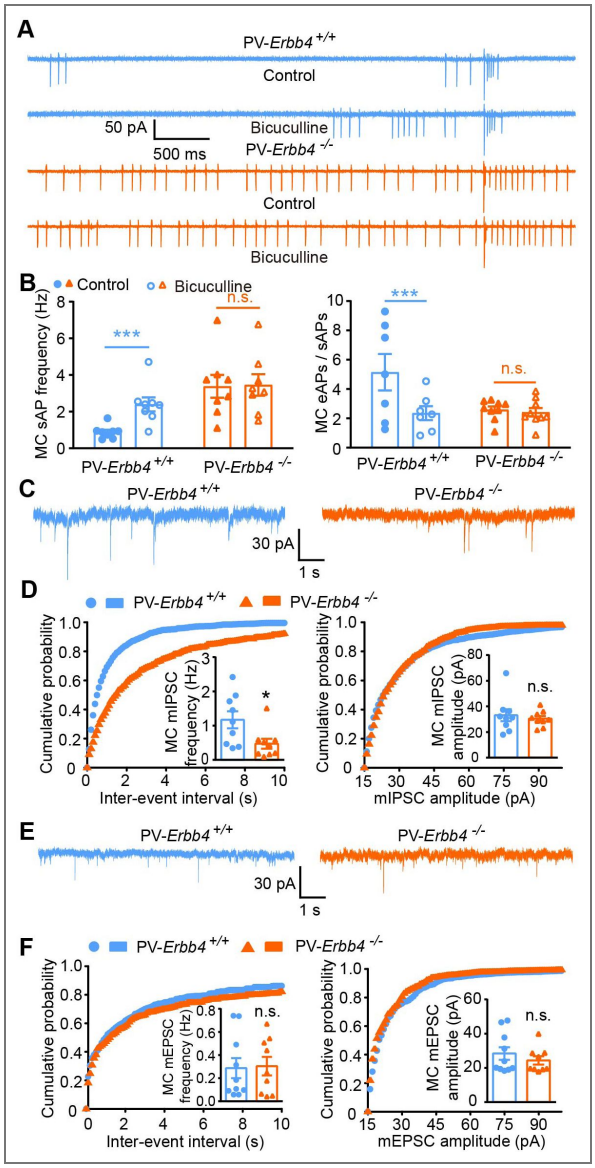


Figure 7. Decreased GABAergic transmission mediates the OB output impairments in PV-*Erbb4*$^{-/-}$ mice.

(A and B) The increased sAP frequency and decreased ratio of eAPs to sAPs in MCs could not be further enhanced by bicuculline in PV-*Erbb4*$^{-/-}$ mice (n = 7 from 3 PV-*Erbb4*$^{+/+}$ mice, n = 9 from 3 PV-*Erbb4*$^{-/-}$ mice; for sAP, $F_{(1,\ 14)}$ = 17.08, P = 0.0008 and 0.5531; for ratio of eAPs to sAPs, $F_{(1,\ 14)}$ = 13.99, P = 0.0007 and 0.9360, two-way ANOVA). (C and D) The frequency but not the amplitude of MC mIPSCs was lower in PV-*Erbb4*$^{-/-}$ mice (n = 9 from 7 PV-*Erbb4*$^{+/+}$and 6 PV-*Erbb4*$^{-/-}$mice; for frequency, $t_{(16)}$ = 2.45, P = 0.0263; for amplitude, $t_{(16)}$ = 0.53, P = 0.6038, unpaired t test). (E and F) Neither frequency nor amplitude of MC mEPSCs was different in PV-*Erbb4*$^{-/-}$ mice versus PV-*Erbb4*$^{+/+}$mice (n = 10 from 5 PV-*Erbb4*$^{+/+}$ mice, n = 9 from 7 PV-*Erbb4*$^{-/-}$ mice; for frequency, $t_{(17)}$ = 0.14, P = 0.8899; for amplitude, $t_{(17)}$ = 0.89, P = 0.3863, unpaired t test). Data are presented as means ± s.e.m. * P < 0.05, *** P < 0.001, **** P < 0.0001, n.s. = not significant.

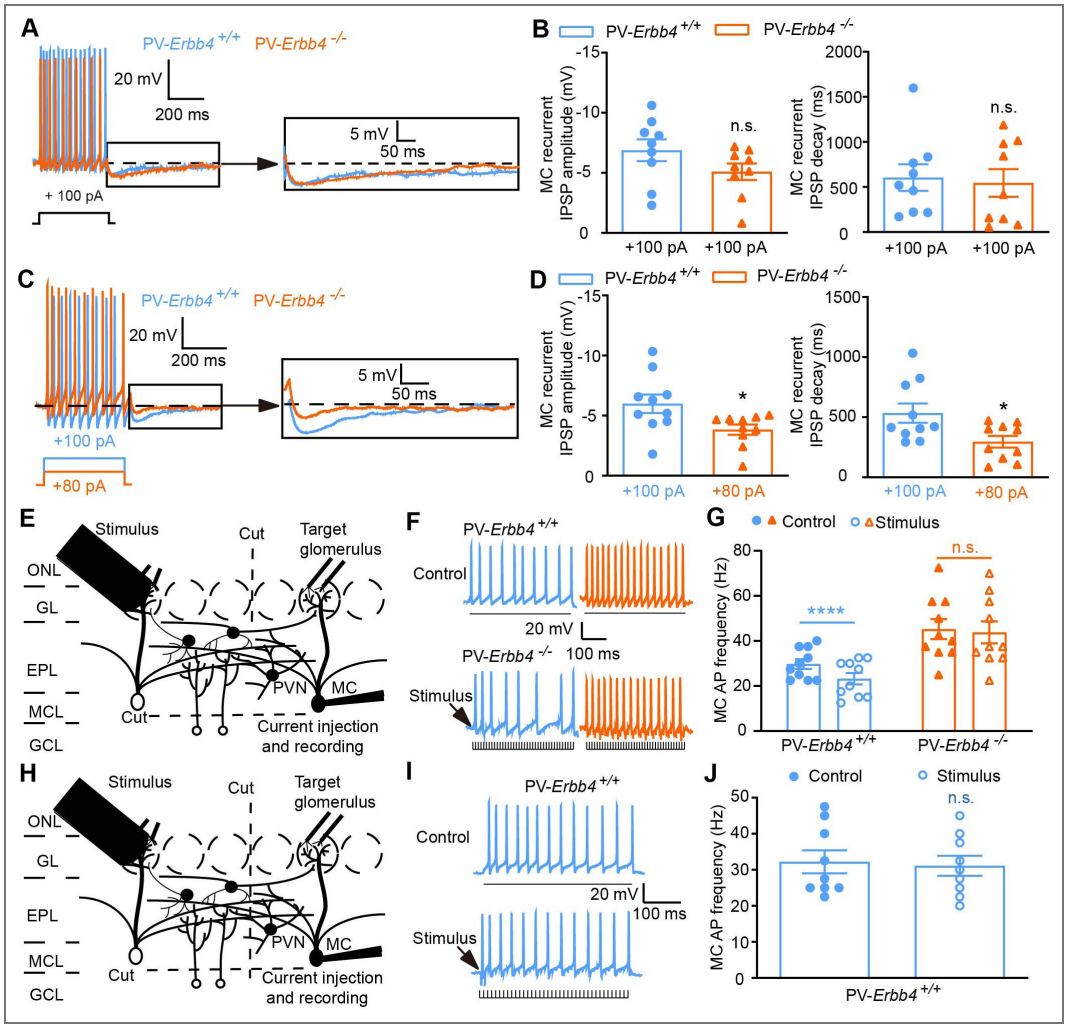


Figure 8. Reduced recurrent inhibition and EPL lateral inhibition of MCs in PV-*Erbb4*$^{-/-}$ mice.

(A and B) Recurrent inhibition did not increase alongside MC hyperactivity in PV-*Erbb4*$^{-/-}$ mice (n = 9 from 5 and 6 mice; for peak amplitude, $t_{(16)}$ = 1.57, P = 0.1351; for decay time constant, $t_{(16)}$ = 0.28, P = 0.7821, unpaired t test). (C and D) Recurrent IPSPs elicited by the same number of MC APs were smaller in PV-*Erbb4*$^{-/-}$ mice. In PV-*Erbb4*$^{-/-}$ mice, an 80 pA current induced ten APs, whereas in PV-*Erbb4*$^{+/+}$ mice, a 100 pA current was needed to induce ten APs. Both the peak amplitude (n = 10 from 6 and 5 mice, $t_{(18)}$ = 2.46, P = 0.0242, unpaired t test) and the decay time constant ($t_{(18)}$ = 2.56, P = 0.0198, unpaired t test) of IPSPs evoked by the same number of APs were reduced in PV-*Erbb4*$^{-/-}$ mice. (E) Schematic of the EPL lateral inhibition experimental configuration. Whole-cell recording of an MC (right side of the schematic) upon stimulus of an adjacent glomerulus (left side of the schematic). A cut was made through the GL and GCL between the sites of conditioning stimulation and target glomerulus to isolate EPL lateral inhibition. (F and G) EPL lateral inhibition was observed in the OB of PV-*Erbb4*$^{+/+}$ mice but not PV-*Erbb4*$^{-/-}$ mice (n = 10 from 7 PV-*Erbb4*$^{+/+}$mice, $F_{(1, 18)}$ = 26.48, P < 0.0001; n = 10 from 6 PV-*Erbb4*$^{-/-}$ mice, P = 0.3426, two-way ANOVA). (H-J) Cutting through the EPL as well abolished the EPL lateral inhibition in PV-*Erbb4*$^{+/+}$ mice. (H) Schematic of the experimental configuration. (I and J) Representative and quantitative analysis of spike frequency in PV-*Erbb4*$^{+/+}$mice (n = 9 from 5 mice, $t_{(8)}$ = 0.80, P = 0.4468, paired t test). EPL, external plexiform layer; GL, glomerular layer; GCL, granule cell layer; MCL, mitral cell layer; ONL, olfactory nerve layer; PVN, PV interneuron. Data are presented as means ± s.e.m. * P < 0.05, **** P < 0.0001, n.s. = not significant.

ErbB4 in OB PV interneurons regulates PV-MC inhibitory synaptic transmission and olfactory behaviours

Finally, we evaluated the contribution of PV-ErbB4 in the OB to olfactory behaviour. ErbB4 expression in the PV interneurons in the OB was largely diminished after *loxP*-flanked *Erbb4* mice were stereotactically injected into the OB with AAV-PV-Cre recombinants, but not when injected with control AAV-PV-GFP (Figure 9A-9C).

ErbB4 reduction in the OB PV interneurons impaired the behavioural discrimination of complex odour mixtures in the reinforced go/no-go task (Figure 9D). Spontaneous dishabituation responses were also impaired in AAV-PV-Cre mice compared with those in the control AAV-PV-GFP group (Figure 9E and 9F). Olfactory detection thresholds for isoamyl acetate and limonene showed a slight increase in AAV-PV-Cre mice compared to AAV-PV-GFP mice (Figure 9G and 9H). Thus, ErbB4 signalling in the PV interneurons in the OB is required for olfactory discrimination and dishabituation in mice.

To directly investigate the effect of ErbB4 signalling on PV-to-MC inhibitory synaptic transmission in OB PV interneurons, we performed optogenetic experiments combined with slice electrophysiology (Figure 9, Supplementary Figure 1A). We stereotaxically injected a 1:1 viral cocktail consisting of AAV-PV-Cre and AAV-EF1α-DIO-hChR2-mCherry into the OB of *loxP*-flanked *Erbb4* mice and wild-type (Wt) control mice to express ChR2 in PV interneurons specifically, and conducted voltage-clamp recordings 10 weeks post-injection. First, we validated reliable ChR2 function in PV interneurons: 473-nm light stimulation (3-s continuous illumination or 10-ms pulses at 1, 5, and 20 Hz) evoked robust photocurrents (Figure 9, Supplementary Figure 1 B), and these responses showed a graded dependence on light intensity (1–3 mW; Figure 9, Supplementary Figure 1C), confirming the effective optogenetic activation of PV interneurons. To verify whether PV interneurons exert inhibitory control over MCs via direct synaptic connections, we performed slice electrophysiological recordings in which PV interneurons were optogenetically activated and postsynaptic currents in MCs were monitored under sequential pharmacological treatments. Application of tetrodotoxin (TTX) completely abolished light-evoked postsynaptic currents in MCs, and subsequent co-administration of TTX and 4-aminopyridine (4-AP, 100 μM) restored these responses, confirming that the recorded currents originated from direct monosynaptic connections between PV interneurons and MCs rather than polysynaptic network activity (Figure 9, Supplementary Figure 1D and 1E). Furthermore, bath application of the $GABA_A$ receptor antagonist bicuculline fully blocked light-evoked postsynaptic currents in MCs, demonstrating that synaptic transmission between PV interneurons and MCs is GABAergic (Figure 9, Supplemental Figure 1D and 1E). Collectively, these findings establish that OB PV interneurons form direct inhibitory synaptic connections with MCs, thereby shaping the OB olfactory circuit output. Critically, recordings from postsynaptic MCs revealed that optogenetic activation of PV interneurons induced significantly weaker light-evoked inhibitory postsynaptic currents (oIPSCs) in *loxP*-flanked *Erbb4* mice than in controls, especially across graded light intensities (Figure 9, Supplemental Figure 1F and 1G). Further analysis of the paired-pulse ratio (PPR, 100-ms inter-pulse interval) showed a significant increase in *loxP*-flanked *Erbb4* mice (Figure 9, Supplementary Figure 1H and 1I), suggesting a reduced presynaptic neurotransmitter release probability. Collectively, these optogenetic data demonstrate that ErbB4 in OB PV interneurons supports their inhibitory synaptic output to MCs, which is associated with presynaptic release efficiency.

Discussion

ErbB4 expression is confined to PV interneurons in the cortex, hippocampus, basal ganglia, and amygdala (Bean et al., 2014; Fazzari et al., 2010) and plays a role in mood (Chen et al., 2022; Chung et al., 2018; Y. Huang et al., 2021) and cognitive behaviours (Cai and Shuman, 2022; Dominguez et al., 2019; Xu et al., 2022). In the present study, we explored the distribution of ErbB4 in OB microcircuits and its functional properties in olfactory behaviour. We found that ErbB4-positive neurones are distributed in all layers of the OB and co-localised with PV interneurons in the IPL and EPL. Furthermore, ErbB4 in PV interneurons regulates OB oscillations

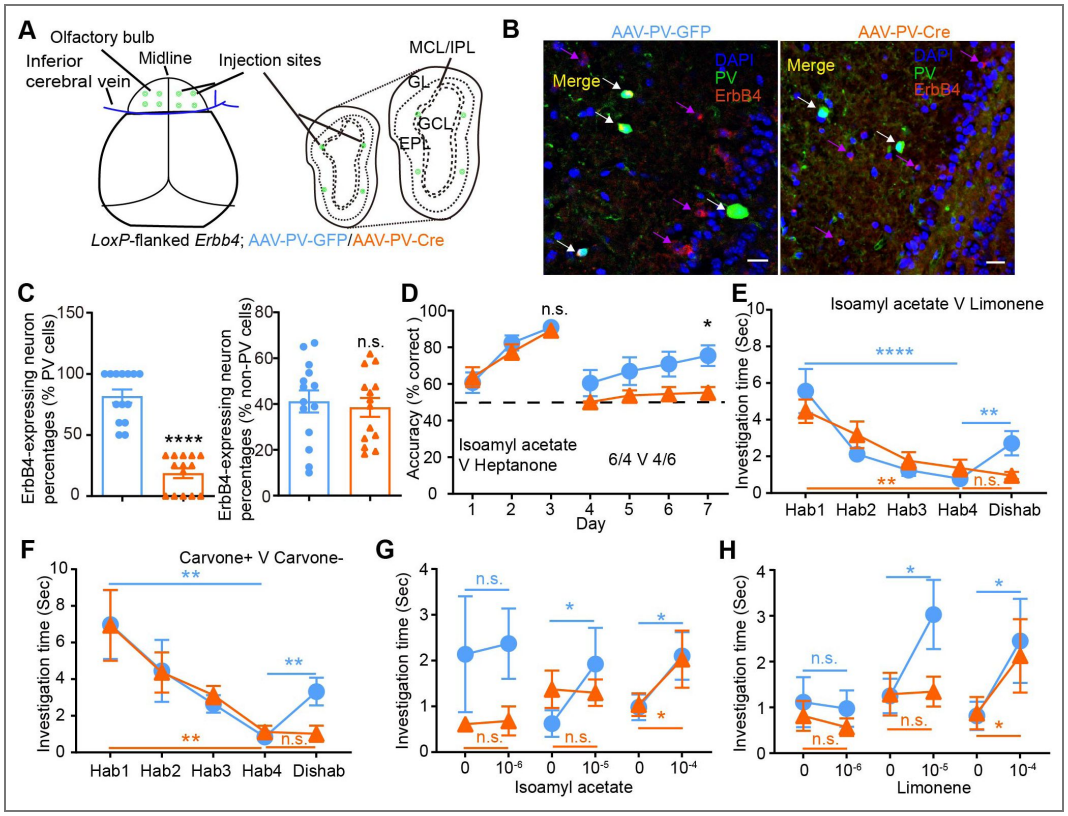


Figure 9. ErbB4 in PV interneurons of the OB is critical for odour discrimination and sensitivity.

(A) Schema indicating virus-injection sites. To specifically delete ErbB4 protein in the PV interneurons of the OB, AAV-PV-Cre was injected into the bilateral OB of neonatal *loxP*-flanked *Erbb4* mice. (B and C) Specific deletion of ErbB4 in PV interneurons (white arrow) but not in non-PV cells (purple arrow) of the OB. OB sections from AAV-PV-GFP injected and AAV-PV-Cre injected mice were stained with DAPI, anti-PV and ErbB4 antibody. Scale bars represent 20 μm. n = 14 slices from 4 mice per group, $t_{(26)}$ = 9.30, P < 0.0001 for PV interneurons, $t_{(26)}$ = 0.41, P = 0.6833 for non-PV cells, unpaired t test. (D) The accuracy in discriminating simple odour pairs was similar for the two groups (n = 6 and 7 mice, $F_{(1, 11)}$ = 0.06, P = 0.8147). The accuracy in discriminating difficult odour pairs was significantly lower in AAV-PV-Cre mice ($F_{(1, 11)}$ = 5.74, P = 0.0355, two-way ANOVA). (E) Both animal groups habituated to isoamyl acetate (n = 10 mice per group, $F_{(3, 54)}$ = 20.94, P < 0.0001 and = 0.0010, two-way ANOVA). However, the AAV-PV-GFP ($F_{(1, 18)}$ = 3.95, P = 0.0045), but not the AAV-PV-Cre mice (P = 0.7107, two-way ANOVA), dishabituated to limonene. (F) Both animal groups habituated to carvone+ (n = 10 mice per group, $F_{(3, 54)}$ = 9.92, P = 0.0019 and 0.0035, two-way ANOVA). However, AAV-PV-GFP ($F_{(1, 18)}$ = 6.72, P = 0.0025), but not AAV-PV-Cre mice (P = 0.9845, two-way ANOVA), dishabituated to carvone-. (G) AAV-PV-GFP mice were able to detect isoamyl acetate at a concentration of 10^{-5} (n = 10 mice, $F_{(1, 18)}$ = 0.04, 2.63 and 12.42, P = 0.8309, 0.0258, and 0.0164 for 10^{-6}, 10^{-5}, and 10^{-4}, two-way ANOVA), whereas AAV-PV-Cre mice only detected isoamyl acetate at a concentration of 10^{-4} (n = 10 mice, P = 0.9484, 0.8930, and 0.0312, two-way ANOVA). (H) AAV-PV-GFP mice detected limonene at 10^{-5} (n = 10 mice, $F_{(1, 18)}$ = 0.28, 3.81 and 11.79, P = 0.7894, 0.0154, and 0.0131 for 10^{-6}, 10^{-5}, and 10^{-4}, two-way ANOVA) but AAV-PV-Cre mice only detected limonene at a higher concentration of 10^{-4} (n = 10 mice, P = 0.6408, 0.9349, and 0.0496 for 10^{-6}, 10^{-5}, and 10^{-4}, two-way ANOVA). Data are presented as means ± s.e.m. * P < 0.05, ** P < 0.01, **** P < 0.0001, n.s. = not significant. EPL, external plexiform layer; GCL, granule cell layer; GL, glomerular layer; IPL, internal plexiform layer; MCL, mitral cell layer.

and odour-evoked output by maintaining GABA release and lateral and recurrent inhibition of MCs. ErbB4 in the OB as a whole or specifically in the PV interneurons contributes to olfactory behavioural performance. Our findings provide evidence that PV interneurons regulate the activity of MC inhibitory neurotransmission and broad ongoing fluctuations, and hence, the olfactory behaviours of discrimination and dishabituation, via ErbB4 signalling.

We found that ErbB4 in the OB is necessary for odour discrimination and dishabituation. In the EPL and IPL, ErbB4 mRNA and protein are primarily localised to PV interneurons. Our data do not rule out ErbB4 expression in other subtypes of interneurons, as suggested by other studies (Bean et al., 2014; Bovetti et al., 2006; Neddens et al., 2011; Tan et al., 2022). ErbB4 in astrocytes and neural precursors affects the distribution and differentiation of interneurons in mature OB and olfactory abilities (Anton et al., 2004; Moy et al., 2009). ErbB4 regulation of interneuron migration relies on a critical time window (prior to E13.5) (Batista-Brito et al., 2023; Mei and Nave, 2014). The late-onset ErbB4 mutation in the OB may not have been sufficient to cause the developmental phenotypes observed with early gene deletion.

PV interneurons are predominantly excited by Ca^{2+}-permeable GluA2-lacking AMPA receptors in the OB and provide strong inhibitory input to MCs (Kato et al., 2013). In the prefrontal cortex, PV interneuron ErbB4 is responsible for the excitatory synaptic plasticity of AMPA and olfactory associative reversal learning (Cai and Shuman, 2022; Xu et al., 2022). Furthermore, transsynaptic binding of ErbB4–Neurexin1β is critical for the activation of ErbB4, extracellular signal-regulated kinase (ERK) 1/2, as well as brain-derived neurotrophic factor (BDNF) in PV interneurons (Cai and Shuman, 2022; Xu et al., 2022). In the OB, Neurexin1β is highly expressed in M/TCs and regulates inhibitory synaptic transmission (Wang et al., 2021). Thus, at the molecular level, the association of ErbB4 with Neurexin1β may facilitate the formation of GluA2-lacking AMPA receptor synapses onto OB PV interneurons, thus regulating GABA release and olfactory processes.

We report here that ErbB4 in PV interneurons most likely regulates the odour detection threshold by reducing background noise and enhancing the SNR of MC responses in the OB. In the neocortex, PV interneurons are implicated in the formation of gamma oscillations, which reduce circuit noise and amplify circuit signals (Sohal et al., 2009). The selective deletion of ErbB4 from fast-spiking PV interneurons increases gamma oscillations in the hippocampus (Del Pino et al., 2013). Our data suggest that ErbB4 in PV interneurons broadly regulates olfactory-related functions by tuning all the frequency bands of ongoing oscillations in the OB. Gamma oscillations in the OB are critical for odour discrimination (Lepousez and Lledo, 2013) and the generation of gamma rhythms in the OB requires inhibitory synaptic transmission in the EPL (Lagier et al., 2004; Lepousez and Lledo, 2013). ErbB4 deficiency in PV interneurons disrupts gamma rhythms by reducing inhibitory synaptic transmission in the OB, leading to the impaired odour discrimination observed in the present study.

The spontaneous activity of MCs is mainly driven by inhibitory interneurons rather than excitatory olfactory sensory neurons (Duchamp-Viret and Duchamp, 1993; Hu et al., 2021; Hu et al., 2017; Stakic et al., 2011). We observed decreases in mIPSC frequency, recurrent inhibition, and lateral inhibition in PV-*Erbb4*$^{-/-}$ mice, suggesting that ErbB4 in PV interneurons plays an important role in regulating M/TC activity through recurrent and lateral inhibitory mechanisms. Another interesting finding was that changes in the spontaneous firing rate differed for odour-evoked excitatory and inhibitory responses *in vivo*, suggesting that ErbB4 in PV interneurons dynamically regulates the spontaneous activity of M/TCs in response to different odours. This result reveals a dual regulatory role of ErbB4 in PV interneurons in olfactory coding. For odour-evoked excitatory responses, PV interneurons (via ErbB4) constrain M/TC spontaneous firing at a low baseline, minimising background noise and enhancing the SNR. In contrast, the inhibitory responses maintain a higher spontaneous firing baseline to accentuate odour-evoked suppression. This regulation amplifies the “excitation of excited M/TCs and inhibition of inhibited M/TCs,” a hallmark of the OB’s “winner-take-all” mechanism that sharpens odour identity coding,

which is critical for odour discrimination. These data confirm that ErbB4 in PV interneurons does not exert a global modulation, but dynamically tailors M/TC spontaneous activity to odour-evoked responses, thereby optimising the ability of the OB to resolve olfactory cues.

In the present study, we identified a spatially broad (300–400 μm in our experiments) lateral inhibitory circuit in the OB that requires ErbB4 in PV interneurons. Thus, our findings suggest that distinct classes of interneurons mediate interglomerular lateral inhibition in different spatial dimensions. For example, short-axon cells usually have relatively long axonal arbours, spanning as much as 1000 μm (Aungst et al., 2003), that may effectively mediate the broadest (up to 600 μm) spatial dimension of lateral inhibition (Whitesell et al., 2013). In contrast, GCs connect only to their neighbouring MCs (< 50–100 μm apart); their lateral inhibition is narrowly tuned (Miyamichi et al., 2013). Moreover, here we found that PV interneurons mediate spatially moderate (300–400 μm) lateral inhibition via ErbB4. Future studies could benefit from defining the functions (e.g. contrast enhancement) of these distinct spatial dimensions of lateral inhibition in odour information processing. Both recurrent and lateral inhibition implement a "winner-takes-all" mechanism: once the strongest input excites the principal cells, firing in the remaining inputs is inhibited (de Almeida et al., 2009; Espinoza et al., 2018; Karmakar and Sarkar, 2013). The regulation of recurrent and lateral inhibition by ErbB4 sheds light on how PV interneurons mediate this "winner-takes-all" inhibitory microcircuit.

In recent decades, impaired odour discrimination has been observed in the earliest stages of neurodegenerative disorders, such as Alzheimer's and Parkinson's diseases (Dan et al., 2021). Olfactory discrimination deficits develop prior to neuropsychological characteristics in patients with Alzheimer's disease and have significant predictive value for future cognitive decline in healthy aging individuals (Carnemolla et al., 2020; Sohrabi et al., 2012; Uchida et al., 2020; Yoshitake et al., 2022). *ErbB4* has been independently identified as a susceptibility gene for Alzheimer's disease and schizophrenia (Mei and Nave, 2014; Swaminathan et al., 2012). Here, we showed that the selective loss of ErbB4 in OB PV interneurons impairs olfactory behaviour. Although ongoing fluctuations predict behavioural alterations in health and disease, the contributions of their different frequency bands remain poorly understood (Iemi et al., 2022). As referenced by Iemi et al. (2022), "fluctuation status" herein refers to the spontaneous, endogenous fluctuations in neural activity that occur in the brain prior to sensory stimulation (i.e. pre-stimulus) or in the absence of external sensory input. External cues do not drive this state but arise from intrinsic neural dynamics, and it is primarily characterised by changes in the power of neural oscillations across multiple frequency bands (e.g., alpha, beta, and their neighbouring frequencies, collectively termed "alpha+ band" in Iemi et al. (2022)). Critically, this fluctuation status is distinct from stimulus-evoked neural responses; it reflects a pre-existing "baseline" state of the neural system that modulates subsequent sensory processing and behaviour. Consistent with Iemi et al. (2022), previous work has established that such ongoing neural fluctuations strongly predict behavioural variability in both health (e.g. slower reaction times and reduced perceptual accuracy) and disease (e.g. age-related cognitive decline and schizophrenia) by regulating neuronal excitability. In our study, we extended this concept to olfactory function, focusing on "broad ongoing fluctuations" (encompassing multiple frequency bands) and linking their dynamics to OB output. Specifically, these fluctuations influence the ability of the OB to support rapid recovery from olfactory adaptation and to mediate complex odour discrimination, thereby uncovering a novel role for endogenous neural fluctuation status in olfactory circuit function. This study links the broad, ongoing fluctuations to OB output and, hence, controls rapid recovery from olfactory adaptation and complex odour discrimination. Our findings will help us better understand the molecular and cellular mechanisms underlying early olfactory dysfunction in neurodegenerative diseases and schizophrenia and provide a potential strategy for treatment.

In summary, our study demonstrates the crucial role of ErbB4 in olfactory behaviours involving ErbB4-expressing PV interneurons. Our results are most likely attributable to presynaptic impairments in inhibitory microcircuits of the OB, which affect odour processing information and lead to abnormal output signals from the M/TCs. The data presented may be promising not only for

understanding the physiological functions of ErbB4 in the OB, but also for providing early diagnosis of Alzheimer's disease and schizophrenia and potential therapeutic applications, particularly in patients with olfactory disorders.

Materials and methods

Reagents and animals

Rabbit polyclonal anti-ErbB4 antibody (sc-283; Santa Cruz Biotechnology, Dallas, TX, USA) was used at dilutions of 1:2,000 for immunoblotting and 1:100 for immunostaining. Rabbit polyclonal anti-ErbB4 antibody (19943-1-AP; Proteintech, Rosemont, IL, USA) was diluted 1:100 for immunostaining, while rabbit monoclonal anti-ErbB4 antibody (#4795; Cell Signalling Technology, Danvers, MA, USA) was used at 1:1000 for immunoblotting. Mouse monoclonal anti-phosphotyrosine antibody (05-321; Sigma-Aldrich, St. Louis, MO, USA) was applied at 0.5 μg per 200 μg total protein for immunoprecipitation, and mouse monoclonal anti-parvalbumin (PV) antibody (P3088; Sigma-Aldrich) was diluted 1:7000 for immunostaining. Anti-β-actin antibody (#4970; Cell Signalling Technology) served as the loading control at 1:5000 dilution for immunoblotting. Goat anti-rabbit IgG conjugated to Alexa Fluor 488 (A11089; Invitrogen, Waltham, MA, USA) and goat anti-mouse IgG conjugated to Alexa Fluor 594 (A11037; Invitrogen) secondary antibodies were both used at 1:400 for immunostaining. The sodium channel blocker tetrodotoxin (TTX, 1069; Tocris, Bristol, United Kingdom) and $GABA_A$ receptor antagonist (+)-bicuculline (ALX-550-515; Enzo Life Sciences, Farmingdale, NY, USA) were obtained from the listed suppliers. All remaining chemicals were purchased from Merck (Sigma– Aldrich).

PV-*Erbb4*$^{-/-}$ were generated by crossing PV-Cre mice with *loxP*-flanked *Erbb4* mice, while PV-*Erbb4*$^{+/+}$ mice carried the PV-Cre transgene and the Wt *Erbb4* allele (Garcia-Rivello et al., 2005; Wen et al., 2010; Xu et al., 2022). The mice were housed under a 12-h light/dark cycle and had ad libitum access to water and food, except during the behavioural tests. All experiments were performed on both sexes of mice. All experimental procedures were conducted in accordance with the guidelines described in the revised Regulations for the Administration of Affairs Concerning Experimental Animals (2011) in China, and were approved by the local Institutional Animal Care and Use Committee.

Immunoprecipitation

Protein samples were resuspended in immunoprecipitation (IP) buffer supplemented with 50 mmol/L HEPES, 150 mmol/L NaCl, 1 mmol/L $ZnCl_2$, 1.5 mmol/L $MgCl_2$, 10% glycerol, 1% Triton X-100, 0.5% Nonidet P-40, and phosphatase/protease inhibitors (Xu et al., 2022). The samples were then incubated with the appropriate primary antibodies at 4 °C overnight, followed by incubation with Protein A Sepharose CL-4B beads (GE Healthcare Biosciences, Uppsala, Sweden) for 2 h at 4 °C with gentle rotation. Immune complexes were collected by centrifugation, and after three sequential washes with IP buffer, bead-bound proteins were eluted and subjected to immunoblotting.

Western blot analysis

Tissues were homogenised in the homogenisation buffer containing 50 mM Mops (pH 7.4), 320 mM sucrose, 100 mM KCl, 0.5 mM $MgCl_2$, 0.2 mM dithiothreitol, and phosphatase and protease inhibitors. Homogenates were resolved by 7.5% SDS/PAGE and transferred to nitrocellulose membranes (Millipore, Billerica, MA, USA), which were blocked with 3% bovine serum albumin (BSA) in Washing buffer (100 mM NaCl, 0.1% Tween-100, 10 mM Tris, pH 7.5). Membranes were incubated overnight with the primary antibody in 1% BSA and then probed with the secondary antibody for 1 h. Signals were visualised using the Immobilon Western Chemiluminescent horseradish peroxidas substrate. Immunoblotting was performed using ImageJ software (National Institutes of Health, Bethesda, MD, USA).

Virus injections

Viral injections were performed as described previously (Kato et al., 2013). Neonatal *loxP*-flanked *Erbb4* mice (0–3 days old) were cryoanesthetized in an ice-cold chamber and head-fixed using a stereotaxic device (RWD68513; RWD Life Science, Shenzhen, China). Viruses driven by the CAG promoter, including pAOV-CAG-EGFP-T2A-Cre (catalog No. CN396, serotype AAV2/8) and pAOV-CAG-EGFP-2A (catalog No. CN394, serotype AAV2/8) were purchased from Obio Technology, Shanghai, China. Additional recombinant adeno-associated viruses, namely rAAV-fPV-CRE-bGH polyA (PT-0275), rAAV-PV-EGFP-bGH polyA (PT-0154) and rAAV-EF1α-DIO-hChR2(H134R)-mCherry-WPRE-hGH polyA (PT-0002, all serotype AAV2/9), were obtained from BrainVTA, Wuhan, China. And the titre was 10^{12} genome copies/mL. For optogenetic activation of OB PV interneurons, a viral cocktail (1:1) of AAV-PV-CRE and AAV-EF1α-DIO-hChR2-mCherry was stereotactically injected into the OB of *loxP*-flanked *Erbb4* or control mice. The injection coordinates were as follows (anteroposterior, mediolateral, and dorsoventral relative to the intersection of the midline and the inferior cerebral vein, in mm): (+0.2, ±0.3, − 0.9/0.7), (+0.2, ±0.6, −0.9/0.7), (+0.5, ±0.3, −0.7/0.5) and (+0.5, ±0.6, −0.7/0.5). The virus (20 nL per site) was injected at a rate of 23 nL/s using a glass pipette. Behavioural tests were performed 10 weeks after the virus injection.

Behavioural analysis

Behavioural analysis was performed by investigators blinded to the experimental animals' genotypes.

Go/no-go test

Mice were deprived of water, allowed to explore the setup (Thinkerbiotech, Nanjing, China), and learned to lick a metal tube just below the odour port to obtain water, as previously described (Hu et al., 2021). The mice self-initiated the trials by poking their noses into the sampling port, which interrupted the infrared light beam. All odours were diluted to 0.01% in mineral oil and further diluted to 1:20 in air using olfactometers. Odour pairs were presented for 2 s in randomised order 0.5 s after trial initiation. Prior to training on the go/no-go task, the mice were trained on the go/go task for 2 days. During the go/go task, if the mice licked within the odour presentation period when presented with either of the odour pairs, they received a water reward. The go/no-go task was then performed to train the mice to discriminate between a pair of odours in order to receive the water reward. Mice learned to lick the metal tube to receive water in response to the rewarded odour (hit) at the end of the trial (2.5-s total trial duration) and to avoid licking the metal tube for the unrewarded odour (correct rejection). Licking when presented with the unrewarded odour (false alarm) led to no water reward and a timeout of up to 10 s. Performance "accuracy" was calculated as the percentage of correct trials (number of hits and correct rejections) over the total number of trials. The weight of the mice under water restriction was strictly monitored (>85% of the initial body weight) during the entire test. The eight-channel semiautomated olfactometers, data acquisition, and analysis were controlled using computer programs written in LabVIEW and MATLAB.

Habituation/dishabituation test

Odours were presented by placing a cotton swab scented with an odour solution (150 μL, 1:2000, freshly prepared with mineral oil before each experiment) above the floor of the animal's home cage, as previously described (Hu et al., 2021). The mice were familiarised with the first odour in four successive trials (habituation) and then exposed to a novel odour in the fifth trial (dishabituation). Five successive 2-min trials were separated by 2 min. Each trial was videotaped and the swab investigation time was quantified offline. Sniffing behaviour was defined as the time when the mouse had its nose within a 1-cm radius from the surface of the cotton swab. A lack of novel odour discrimination was considered to occur when mice spent as much time investigating the swab during the dishabituation trial as during the fourth habituation trial.

Odour detection threshold test

Odour detection thresholds were obtained according to previously described procedures (Nicolis di Robilant et al., 2019). Odours (isoamyl acetate and limonene) were freshly diluted with mineral oil to different concentrations (10^{-6}, 10^{-5}, and 10^{-4} in 150 µL) and applied to a cotton swab, then placed above the floor of the animal's cage along with mineral oil on the other side. Each trial lasted 2 min with 2-min intertrial intervals. Mice were deemed able to detect the odour when they spent more time sniffing the diluted odour than the mineral oil, and the minimum concentration detected by the mice was taken as the threshold.

Buried food pellet test

All chow pellets were removed from the home cages 24 h before testing. The mice had ad libitum access to water. Before each experimental trial, 10-to 12-week-old mice were familiarised with the test cage for 10 min. In each trial, a single mouse was placed in the test cage (46 × 30 × 16 cm) to recover a 0.2-*g* food pellet buried 0.5 cm below the bedding material surface. Food pellet locations were randomly selected. The time between when the mouse was placed in the cage and when it grasped the food pellet with its forepaws or teeth was recorded and defined as latency. The mice were allowed to consume food pellets and were returned to their cages. The food pellet was presented to the mouse for consumption if it was not found within 300 s, in which case, the latency was recorded as 300 s. A visible food pellet test was conducted as a control. The procedures were identical, except that the pellets were placed randomly on the bedding surface.

RNAscope

To examine the expression of the *Erbb4* gene, RNAscope was performed using an RNAscope Fluorescent Multiplex Kit (Advanced Cell Diagnostics (ACDBio), Newark, CA, USA) according to the manufacturer's recommendations. Briefly, the OB was cut into 20-µm coronal sections. Sections were serially thaw-mounted onto 20 slides (Fisherbrand, Waltham, MA, USA) through the entire OB and then air-dried for 1 h at room temperature prior to storage at −80 °C. RNAscope probes were obtained from ACDBio for *Erbb4* (Cat #318721) and *Pv* (Cat #421931-C2). The sections were counterstained with the nuclear marker DAPI (Cat #104139, Abcam, Cambridge, United Kingdom). *Erbb4* mRNA intensity in the OB was measured using ZEN Blue 3.0 and ImageJ software. Experimenters blinded to the group assignments performed image collection and subsequent data analysis.

Immunohistochemistry

Mice (4 weeks old) were perfused transcardially with 4% paraformaldehyde (PFA). Dissected brains were postfixed overnight and dehydrated in 30% sucrose for 24 h at 4 °C, after which the OBs were cut into 40-µm-thick horizontal sections on a vibratome (Leica Microsystems, Wetzlar, Germany). OB sections were processed for double immunofluorescence in 0.1 M PBS (pH 7.4) as follows: three washes in 0.1 M PBS, 10 min each; blocking in 0.1 M PBS containing 10% normal goat serum, 1% BSA, and 0.25% Triton X-100 overnight at 4 °C; primary antibody incubation for 40 h at 4 °C in blocking solution; three washes; secondary antibody for 90 min at room temperature in blocking solution; three washes; rinsing with PBS and mounting with a mounting medium (Vector Laboratories, Burlingame, CA, USA). Immunoreactivity was assessed using Alexa Fluor 488– and 594-conjugated goat anti-mouse IgG antibodies. Sections were analysed using a confocal microscope (Zeiss LSM710, Carl Zeiss AG, Oberkochen, Germany) at 20× and 60× magnifications. ErbB4 intensity in the OB was measured using ZEN Blue 3.0 and ImageJ software. Cresyl violet staining was performed as described previously. The optimal cutting temperature compound-embedded OBs were cut into 20-µm sections. OB sections were stained with 0.1% cresyl violet for 35 min, dehydrated using ascending grades of alcohol, cleared with xylene, mounted, and observed under an Olympus microscope.

Slice preparation and patch-clamp electrophysiology

Acute OB slices were prepared as described previously (Hu et al., 2021; Hu et al., 2017). Briefly, animals were heavily anaesthetised with ketamine/xylazine (140/20 mg/kg, intraperitoneally) and decapitated. The OB was quickly removed and immersed in ice-cold, and oxygenated (95% O_2/5% CO_2) ACSF containing 124 mM NaCl, 3 mM KCl, 2 mM $CaCl_2$ 1.3 mM $MgCl_2$, 25 mM $NaHCO_3$, 1.25 mM NaH_2PO_4, and 10 mM glucose. Horizontal slices (300 μm) were cut with a VT1000s vibratome (Leica), recovered at 37 °C for 30 min and then maintained at 25 °C.

OB slices were transferred to a recording chamber, which was warmed to 33 °C and superfused with oxygenated ACSF (2 mL/min). Neurones were visualised with infrared optics using an upright microscope equipped with a 60× water-immersion lens (BX51WI; Olympus, Tokyo, Japan) and an infrared-sensitive charge-coupled device camera. MCs and PV interneurons were identified based on their fluorescence, morphology, size, location, and electrophysiological characteristics.

For cell-attached mode, recording pipettes with resistances of 6–8 MΩ were pulled from borosilicate glass capillaries (P97; Sutter Instrument Co., Novato, CA, USA) and filled with ACSF. To record olfactory-nerve-evoked responses, monophasic square pulses (200 μs) with an intensity of 0.2 mA or gradual increasing intensities of 0.1, 0.15, 0.2, 0.25, and 0.3 mA were delivered through a concentric electrode that was placed on the outermost layer of the OB, near the recorded MC. The firing frequency was defined as the number of action potentials/time windows. A 5-s window prior to olfactory nerve stimulation was used to assess the spontaneous firing rate, and the first 1-s window after stimulation of the olfactory nerve was used to assess the evoked response. The signal-to-noise ratio (SNR) was defined as the ratio of evoked responses to spontaneous firing 5 s before the olfactory nerve stimulation.

To record whole-cell action potentials and mEPSCs, pipettes were filled with a solution containing 140 mM K-methylsulfate, 4 mM NaCl, 10 mM HEPES, 0.2 mM EGTA, 4 mM MgATP, 0.3 mM Na_3GTP, and 10 mM phosphocreatine (pH was adjusted to 7.4 with KOH). MCs were held at −65 mV in the presence of 20 μM bicuculline and 1 μM TTX during recording of mEPSCs.

To isolate mIPSCs, MCs were held at −65 mV in the presence of 50 μM AP5, 20 μM NBQX and 1 μM TTX with a CsCl-base intracellular solution containing (mM): 135 CsCl, 10 HEPES, 0.2 EGTA, 2 Na_2ATP, 0.3 Na_3GTP, and 10 glucose.

Lateral inhibition recordings were performed as previously described (Arevian et al., 2008; Hu et al., 2017; Whitesell et al., 2013). Briefly, a concentric bipolar stimulating electrode was placed into the caudal glomerulus located 3–4 glomeruli (~400 μm) caudally from the one correlated with the recorded MC. The intensity of the stimulation was moderate (100 μA) to avoid stimulating the glomerulus of the recorded MC, which would invariably evoke excitatory postsynaptic potentials (EPSPs). Pulses of 200-μs duration were delivered at 100 Hz and synchronised with the recording using a Master-8 stimulator (A.M.P.I., Jerusalem, Israel). Alexa 488 dye (100 μM) was added to the intracellular solution to visualise cell morphology.

Photostimulation (273 nm, 10-ms pulses) of ChR2-expressing PV interneurons was delivered through an optical fibre placed near the slice and connected to an intelligent optogenetic system (Aurora-220; NEWDOON, Hangzhou, China). Photostimulation was triggered using Clampex software (Molecular Devices, San Jose, CA, USA). During optogenetic experiments, PV interneurons were voltage-clamped at –70 mV, while MCs were maintained at a holding potential of 0 mV.

Signals were acquired with a MultiClamp 700 B amplifier (Molecular Devices), filtered at 2 kHz, and sampled at 10 kHz using a Digidata 1440A interface (Molecular Devices) and Clampex 10.2 software (Molecular Devices). The data were accepted when the series resistance remained within 15% of the initial value. Miniature events in a 5-min recording period were analysed using the Mini Analysis software (version 6.07; Synaptosoft, Decatur, GA, USA).

Single-cell RT-PCR

At the end of the recording session, gentle suction was applied to aspirate the cytoplasm into the pipette, while maintaining a tight seal. After complete incorporation of the soma, the pipette was carefully removed from the neuron to perform an outside-out patch recording, and then quickly removed from the bath. The harvested contents were transferred into PCR tubes. RT was performed in a final volume of 20 μL using a QuantiTect Reverse Transcription Kit (Cat. No. 205311; QIAGEN, Venlo, The Netherlands). Next, outer and nested primer sets were used for two consecutive rounds of PCR as described previously (Vullhorst et al., 2009). For the first round of PCR, all targets were amplified simultaneously using outer primer pairs for PV and ErbB4 (first set PCR primer sequences: GCCTGAAGAAAAAGAACCCG and AATCTTGCCGTCCCCATCCT for PV, CCAGCC CAGCGCTTCTCAGTCAG and GTATTTCGGTCAGGTTCTTTAATCC for ErbB4, 20 pmol of each) in a final volume of 100 μL for 21 cycles. Each cycle comprised a 94 °C denaturation for 30 s, 60 °C annealing for 30 s, and 72 °C extension for 30 s. For the second round of PCR, PV and ErbB4 were separately reamplified using specific nested primer sets for 35 cycles of PCR, as described above, with 2 μL of the first PCR product as template (second primer sequences: CGGATGAGGTGAAGAAGGTGT and TC CCCATCCTTGTCTCCAGC for PV, CTGACCTGGAACAGCAGTACCGA and AGGCATAGCGATCTTCATATAGT for ErbB4). The products were assayed on 2% agarose gels stained with Gel Red, with dl1000 as the molecular weight marker.

Implantation of electrodes for in vivo electrophysiological recordings

After deep anaesthesia, the mice were secured in a stereotaxic frame. The fur on the scalp surface was removed from the midpoint between the ears and the midline of the orbits. For the spike and LFP recordings, tetrodes (single-wire diameter, item no. PF000591, RO-800, 0.0005”/12.7 μm, coating 1/4 hard PAC, Sandvik AB, Stockholm, Sweden) were implanted into the hole drilled above the OB (4.28 mm anterior from bregma, 1.0 mm lateral from the midline). The electrodes were inserted into the brain after the dura mater was punctured. Each electrode was connected to a 16-channel electrode interface board (EIB-16; Neuralynx, Bozeman, MT, USA). Signals were sent to a headstage, amplified using a 16-channel amplifier (Plexon Inc., Dallas, TX, USA), and monitored in real time to ensure optimal placement within the ventral MC layer. Despite the presence of diverse cell types in the OB, only the spiking activity of M/TCs can be captured via tetrode recordings (Kay and Laurent, 1999; Doucette et al., 2011). A stainless steel screw was inserted into the parietal bone (1 mm posterior to the bregma and 1 mm from the midline) and connected to the ground as the reference electrode. Finally, a custom-designed aluminium head plate was sealed to the skull surface using dental cement to enable head fixation during recording. The mice were returned to their home cages for at least a week.

Electrophysiological recordings in awake mice

Recordings began at least one week after electrode implantation. The mice were head-fixed with two horizontal bars fixed to the headplate using two screws, and were able to walk on an air-supported floating polystyrene foam ball (Thinkerbiotech). For spike recordings, the signals from the electrodes were filtered at 300–5000 Hz and sampled at 40 kHz. Odour stimulus event markers were recorded alongside the spike recording. For LFP recordings, the signals were amplified by a 2000× gain, bandpass filtered (0.1–300 Hz, and sampled at 1 kHz (Plexon Inc.).

Odour application for electrophysiological recordings in awake mice

A standardised panel of eight odours (isoamyl acetate, 2-heptanone, phenyl acetate, benzaldehyde, dimethylbutyric acid, n-heptane acid, n-pentanol, and 2-pentanone; purchased from Sinopharm Chemical Reagent Co., Ltd., Beijing, China) was prepared using an odour delivery system (Thinkerbiotech). Charcoal-filtered air was supplied to the mouse nose at a constant rate of 1 L/min to eliminate airflow interference. This method has been validated in previous studies to

effectively limit odour stimulation to within 2 s. All odours were dissolved in a 1% (v/v) dilution of mineral oil. During odour stimulation, a stream of charcoal-filtered air flowed over the oil at a total flow rate of 1 L/min, and the vapour-phase concentration was further diluted by the carrier airflow to 1/20. Mice were first anaesthetised with isoflurane for approximately 20 s and then rapidly transferred to a polystyrene foam ball. Before the start of *in vivo* electrophysiological recordings, the mice were given 10 min to acclimate to the fixation and recover from isoflurane. Odour presentation was controlled using an odour delivery system coupled to a solenoid valve driven by a digital-to-analogue converter. Each odour was presented for 2 s, with an inter-trial interval of approximately 24 s.

Offline spike sorting and statistics of the unit data

Spikes were identified and sorted from the raw data using Offline Sorter V4 software (Plexon Inc.). Spikes were detected and sorted when they had an amplitude exceeded 5 times the noise standard deviation. Principal component analysis of the data was performed to separate the different units. When <0.75% of the inter-spike intervals were <1 ms, the unit was classified as a single unit. Data from 4 s before to 6 s after the onset of the odour stimulation event were extracted, and the spike firing rate was averaged within 100-ms bins to generate a peristimulus time histogram (PSTH). The spontaneous and odour-evoked firing rates were calculated by averaging the spikes recorded during 4–2 s before odour stimulation and 2 s after the start of odour stimulation, respectively. To determine whether the odour evoked a significant response, we used the Wilcoxon signed-rank test to compare the spontaneous (baseline) firing rate with the odour-evoked firing rate across all trials. Unit-odour pairs ($P > 0.05$) were defined as non-responsive; those ($P < 0.05$) were defined as responsive, and responsive pairs were further categorised as excitatory (odour-evoked firing rate > spontaneous firing rate) or inhibitory (odour-evoked firing rate < spontaneous firing rate). Subtracting the baseline firing rate from the odour-evoked firing rate yielded the mean firing rate (MFR). The SNR was defined as the odour-evoked firing rate divided by the baseline firing rate.

LFP signal analysis

The LFP signals were analysed using a MATLAB script and divided into different frequency bands: theta (2–12 Hz), beta (15–35 Hz), low-gamma (36–65 Hz), and high-gamma (66–95 Hz). The spectral power of each frequency resolution was calculated over a 4-s window. The spectral powers of all frequencies within the bandwidth were averaged.

Statistical analysis

Data are presented as the mean ± standard error of the mean (SEM). Unpaired or paired *t* tests were used to compare data between the two groups. The Chi-square test was used to compare the two constituent ratios. One-way or two-way ANOVAs were used to comparemore than two groups (western blot, behavioural, and electrophysiological studies). Tukey's post-hoc adjustment was used for multiple pairwise comparisons in the behavioural tests. All tests were two-sided, and statistical significance was set at $P < 0.05$. Statistical analyses were performed using the GraphPad Prism software.

Data availability

All data generated or analyzed during this study are included in the manuscript and supporting files.

Additional information

Author Contributions

Bin Hu, Data curation, Formal analysis, Funding acquisition, Investigation, Methodology, Writing—original draft; Chi Geng, Data curation, Formal analysis, Investigation, Methodology, Writing—original draft; Feng Guo, Ying Liu, Data curation, Formal analysis, Investigation, Methodology; Ran

Wang, Investigation, Methodology; You-Ting Chen, Methodology; Xiao-Yu Hou, Conceptualization, Resources, Supervision, Funding acquisition, Validation, Project administration, Writing—review and editing.

Ethics

All experimental procedures were conducted in accordance with the guidelines described in the revised Regulations for the Administration of Affairs Concerning Experimental Animals (2011) in China and approved by the local Institutional Animal Care and Use Committee.

Funding

Funder	Grant reference number	Author
MOST | National Natural Science Foundation of China (NSFC)	81673418	Xiao-Yu Hou
MOST | National Natural Science Foundation of China (NSFC)	81701084	Bin Hu
Jiangsu 333 Program	BRA2018059	Xiao-Yu Hou

Author ORCID iDs

Xiao-Yu Hou: https://orcid.org/0000-0001-5409-8785

Additional files

Figure 1 and 2—figure supplement 1. Uncropped western blot images. (A) Uncropped western blot images for p-ErbB4 in Figure 1C. (B) Uncropped western blot images for total ErbB4 in Figure 1C. (C) Uncropped western blot images for ErbB4 in Figure 1F. (D) Uncropped western blot images for ErbB4 in Figure 2K.

Figure 2—figure supplement 2. The overall lamina structures of the OB were not affected in PV-*Erbb4*$^{-/-}$ mice. Cresyl violet staining was performed to examine coronal structure sections of the OB at 2 and 6 months of age. Scale bars represent 200 μm for the overall views and 50 μm for the magnified images. EPL, external plexiform layer; GCL, granule cell layer; GL, glomerular layer; IPL, internal plexiform layer; MCL, mitral cell layer; ONL, olfactory nerve layer.

Figure 4—figure supplement 1. Analysis of M/TC spike waveform features in PV-*Erbb4*$^{+/+}$ and PV-*Erbb4*$^{-/-}$ mice. (A) Separation of the 2 units (red and blue dots) using PCA. (B) Examples of isolated two different single units (unit a, red; unit b, blue). (C) Examples of spike waveform shapes of M/TCs in PV-*Erbb4*$^{+/+}$ and PV-*Erbb4*$^{-/-}$ mice. (D) Quantitative analysis of peak-to-valley ratio of spikes ($t_{(52)}$ = 1.92, P = 0.0610, unpaired t test). (E) Quantitative analysis of half-valley width of spikes ($t_{(52)}$ = 1.41, P = 0.1648, unpaired t test). Data are presented as means ± s.e.m. n.s. = not significant.

Figure 7—figure supplement 1. Electrophysiological properties of OB PV interneurons in PV-*Erbb4*$^{+/+}$ and PV-*Erbb4*$^{-/-}$ mice. (A and B) Reduced frequency and amplitude of OB PV interneuron mEPSCs in PV-*Erbb4*$^{-/-}$mice (n = 6 from 3 PV-*Erbb4*$^{+/+}$mice, n = 4 from 3 PV-*Erbb4*$^{-/-}$ mice; for frequency, $t_{(8)}$ = 2.43, P = 0.0411; for amplitude, $t_{(8)}$ = 3.15, P = 0.0136, unpaired t test). (C) Increased frequency of OB PV interneuron APs in PV-*Erbb4*$^{-/-}$ mice ($t_{(8)}$ = 2.394, P = 0.0436, unpaired t test). (D) Quantitative analysis of AP amplitude in OB PV interneurons ($t_{(8)}$ = 1.52, P = 0.1660, unpaired t test). (E) Quantitative analysis of AP half-width in OB PV interneurons ($t_{(8)}$ = 0.99, P = 0.3528, unpaired t test). Data are presented as means ± s.e.m. * P < 0.05, **** P < 0.0001, n.s. = not significant.

Figure 8—figure supplement 1. Approximately the same AP firing rate elicited by different current intensities across PV-*Erbb4*$^{+/+}$ and PV-*Erbb4*$^{-/-}$ mice. (A) A current injection of ~ 80 pA in PV-*Erbb4*$^{-/-}$ mice elicited approximately the same firing rate as a current injection of ~ 100 pA in PV-*Erbb4*$^{+/+}$ mice (n = 10 from 6 and 5 mice, $t_{(18)}$ = 0.09, P = 0.9316, unpaired t test). Data are presented as means ± s.e.m. n.s. = not significant.

Figure 9—figure supplement 1. ErbB4 deletion in OB PV interneurons attenuates PV interneuron-mediated inhibitory modulation of MCs. (A) Schematic diagram illustrating the experimental paradigm, including stereotaxic virus injection and subsequent slice electrophysiological recordings; blue light illumination was delivered to OB slices, with recordings performed from PV interneurons expressing ChR2 or postsynaptic MCs. (B) Representative voltage-clamp recordings of PV interneuron currents in response to 3-s continuous 473-nm light illumination and pulsed light stimulation (10-ms pulses at 1, 5, and 20 Hz). (C) Representative voltage-clamp traces of PV interneuron currents evoked by graded 473-nm light intensities (1, 2, and 3 mW). (D and E) Representative traces and quantitative analysis of oIPSCs in MCs under distinct pharmacological conditions (Con, TTX, TTX + 4-AP, and bicuculline (Bic)). Statistical comparisons: Con vs. TTX, P = 0.0004; TTX vs. TTX + 4-AP, P < 0.0001; TTX + 4-AP vs. Bic, P < 0.0001 (n = 3 from 3 Wt mice; $F_{(3, 8)}$ = 47.78, one-way ANOVA). (F and G) Representative traces and quantitative analysis of light-evoked MC oIPSCs across graded illumination intensities in Wt and *loxP*-flanked *Erbb4* mice (n = 10 from 3 mice per group; two-way ANOVA, $F_{(1, 53)}$ = 23.26, P < 0.0001). (H and I) Representative traces and quantitative analysis of PPR (100-ms inter-pulse interval) of light-evoked MC oIPSCs in Wt and *loxP*-flanked *Erbb4* mice (n = 10 from 3 mice per group; P = 0.0163, $t_{(18)}$ = 2.651, unpaired t test). Data are presented as means ± s.e.m. * P < 0.05, *** P < 0.001, **** P < 0.0001. EPL, external plexiform layer; GCL, granule cell layer; GL, glomerular layer; IPL, internal plexiform layer; MCL, mitral cell layer; ONL, olfactory nerve layer; PVN, parvalbumin interneuron.

References

1. **Aghvami SS,** Kubota Y, Egger V (2022) Anatomical and functional connectivity at the dendrodendritic reciprocal mitral cell-granule cell synapse: impact on recurrent and lateral inhibition. *Front Neural Circuits* **16**:933201 https://doi.org/10.3389/fncir.2022.933201 | PubMed

2. **Anton ES,** Ghashghaei HT, Weber JL, McCann C, Fischer TM, Cheung ID, Gassmann M, Messing A, Klein R, Schwab MH, *et al.* (2004) Receptor tyrosine kinase ErbB4 modulates neuroblast migration and placement in the adult forebrain. *Nature Neuroscience* **7**:1319-1328 https://doi.org/10.1038/nn1345 | PubMed

3. **Arevian AC,** Kapoor V, Urban NN (2008) Activity-dependent gating of lateral inhibition in the mouse olfactory bulb. *Nature Neuroscience* **11**:80-87 https://doi.org/10.1038/nn2030 | PubMed

4. **Aungst JL,** Heyward PM, Puche AC, Karnup SV, Hayar A, Szabo G, Shipley MT (2003) Centre-surround inhibition among olfactory bulb glomeruli. *Nature* **426**:623-629 https://doi.org/10.1038/nature02185 | PubMed

5. **Batista-Brito R,** Majumdar A, Nuno A, Ward C, Barnes C, Nikouei K, Vinck M, Cardin JA (2023) Developmental loss of ErbB4 in PV interneurons disrupts state-dependent cortical circuit dynamics. *Molecular Psychiatry* **28**:3133-3143 https://doi.org/10.1038/s41380-023-02066-3 | PubMed

6. **Bean JC,** Lin TW, Sathyamurthy A, Liu F, Yin DM, Xiong WC, Mei L (2014) Genetic labeling reveals novel cellular targets of schizophrenia susceptibility gene: distribution of gaba and non-gaba erbb4-positive cells in adult mouse brain. *The Journal of Neuroscience* **34**:13549-13566 https://doi.org/10.1523/JNEUROSCI.2021-14.2014 | PubMed

7. **Bovetti S,** De Marchis S, Gambarotta G, Fasolo A, Perroteau I, Puche AC, Bovolin P (2006) Differential expression of neuregulins and their receptors in the olfactory bulb layers of the developing mouse. *Brain Research* **1077**:37-47 https://doi.org/10.1016/j.brainres.2006.01.034 | PubMed

8. **Cai DJ,** Shuman T (2022) A distinct signaling pathway in parvalbumin-positive interneurons controls flexible memory updating. *Neuropsychopharmacology* **47**:1283-1284 https://doi.org/10.1038/s41386-022-01298-1 | PubMed

9. **Carnemolla SE,** Hsieh JW, Sipione R, Landis BN, Kumfor F, Piguet O, Manuel AL (2020) Olfactory dysfunction in frontotemporal dementia and psychiatric disorders: a systematic review. *Neuroscience and Biobehavioral Reviews* **118**:588-611 https://doi.org/10.1016/j.neubiorev.2020.08.002 | PubMed

10. **Chen YH,** Hu NY, Wu DY, Bi LL, Luo ZY, Huang L, Wu JL, Wang ML, Li JT, Song YL, *et al.* (2022) PV network plasticity mediated by neuregulin1-ErbB4 signalling controls fear extinction. *Molecular Psychiatry* **27**:896-906 https://doi.org/10.1038/s41380-021-01355-z | PubMed

11. **Chung DW,** Chung Y, Bazmi HH, Lewis DA (2018) Altered ErbB4 splicing and cortical parvalbumin interneuron dysfunction in schizophrenia and mood disorders. *Neuropsychopharmacology* **43**:2478-2486 https://doi.org/10.1038/s41386-018-0169-7 | PubMed

12. **Dan X,** Wechter N, Gray S, Mohanty JG, Croteau DL, Bohr VA (2021) Olfactory dysfunction in aging and neurodegenerative diseases. *Ageing Research reviews* **70**:101416 https://doi.org/10.1016/j.arr.2021.101416 | PubMed

13. **de Almeida L,** Idiart M, Lisman JE (2009) A second function of gamma frequency oscillations: an E%-max winner-take-all mechanism selects which cells fire. *The Journal of Neuroscience* **29**:7497-7503 https://doi.org/10.1523/JNEUROSCI.6044-08.2009 | PubMed

14. **Del Pino I,** Garcia-Frigola C, Dehorter N, Brotons-Mas JR, Alvarez-Salvado E, Martinez de Lagran M, Ciceri G, Gabaldón MV, Moratal D, Dierssen M, *et al.* (2013) Erbb4 deletion from fast-spiking interneurons causes schizophrenia-like phenotypes. *Neuron* **79**:1152-1168 https://doi.org/10.1016/j.neuron.2013.07.010 | PubMed

15. **Deng W,** Luo F, Li BM, Mei L (2019) NRG1-ErbB4 signaling promotes functional recovery in a murine model of traumatic brain injury via regulation of GABA release. *Experimental Brain Research* **237**:3351-3362 https://doi.org/10.1007/s00221-019-05680-2 | PubMed

16. **Dominguez S,** Rey CC, Therreau L, Fanton A, Massotte D, Verret L, Piskorowski RA, Chevaleyre V (2019) Maturation of PNN and ErbB4 signaling in area CA2 during adolescence underlies the emergence of PV interneuron plasticity and social memory. *Cell Reports* **29**:1099-1112.e1094. https://doi.org/10.1016/j.celrep.2019.09.044 | PubMed

17. **Doucette W,** Gire DH, Whitesell J, Carmean V, Lucero MT, Restrepo D (2011) Associative cortex features in the first olfactory brain relay station. *Neuron* **69**:1176-1187 https://doi.org/10.1016/j.neuron.2011.02.024 | PubMed

18. **Duchamp-Viret P,** Duchamp A (1993) GABAergic control of odour-induced activity in the frog olfactory bulb: possible GABAergic modulation of granule cell inhibitory action. *Neuroscience* **56**:905-914 https://doi.org/10.1016/0306-4522(93)90136-4 | PubMed

19. **Egger V,** Kuner T (2021) Olfactory bulb granule cells: specialized to link coactive glomerular columns for percept generation and discrimination of odors. *Cell and Tissue Research* **383**:495-506 https://doi.org/10.1007/s00441-020-03402-7 | PubMed

20. **Espinoza C,** Guzman SJ, Zhang X, Jonas P (2018) Parvalbumin(+) interneurons obey unique connectivity rules and establish a powerful lateral-inhibition microcircuit in dentate gyrus. *Nature Communications* **9**:4605 https://doi.org/10.1038/s41467-018-06899-3 | PubMed

21. **Fazzari P,** Paternain AV, Valiente M, Pla R, Lujan R, Lloyd K, Lerma J, Marín O, Rico B (2010) Control of cortical GABA circuitry development by Nrg1 and ErbB4 signalling. *Nature* **464**:1376-1380 https://doi.org/10.1038/nature08928 | PubMed

22. **Garcia-Rivello H,** Taranda J, Said M, Cabeza-Meckert P, Vila-Petroff M, Scaglione J, Ghio S, Chen J, Lai C, Laguens RP, *et al.* (2005) Dilated cardiomyopathy in Erb-b4-deficient ventricular muscle. *American Journal of Physiology-Heart and Circulatory Physiology* **289**:H1153-H1160 https://doi.org/10.1152/ajpheart.00048.2005 | PubMed

23. **Grieco SF,** Wang G, Mahapatra A, Lai C, Holmes TC, Xu X (2020) Neuregulin and ErbB expression is regulated by development and sensory experience in mouse visual cortex. *The Journal of Comparative Neurology* **528**:419-432 https://doi.org/10.1002/cne.24762 | PubMed

24. **Gschwend O,** Abraham NM, Lagier S, Begnaud F, Rodriguez I, Carleton A (2015) Neuronal pattern separation in the olfactory bulb improves odor discrimination learning. *Nature Neuroscience* **18**:1474-1482 https://doi.org/10.1038/nn.4089 | PubMed

25. **Hu B,** Geng C, Guo F, Liu Y, Zong YC, Hou XY (2021) GABAA receptor agonist muscimol rescues inhibitory microcircuit defects in the olfactory bulb and improves olfactory function in APP/PS1 transgenic mice. *Neurobiology of Aging* **108**:47-57 https://doi.org/10.1016/j.neurobiolaging.2021.08.003 | PubMed

26. **Hu B,** Geng C, Hou XY (2017) Oligomeric amyloid-β peptide disrupts olfactory information output by impairment of local inhibitory circuits in rat olfactory bulb. *Neurobiology of Aging* **51**:113-121 https://doi.org/10.1016/j.neurobiolaging.2016.12.005 | PubMed

27. **Huang L,** Garcia I, Jen HI, Arenkiel BR (2013) Reciprocal connectivity between mitral cells and external plexiform layer interneurons in the mouse olfactory bulb. *Frontiers in Neural Circuits* **7**:32 https://doi.org/10.3389/fncir.2013.00032 | PubMed

28. **Huang Y,** Jiang H, Zheng Q, Fok AHK, Li X, Lau CG, Lai CSW (2021) Environmental enrichment or selective activation of parvalbumin-expressing interneurons ameliorates synaptic and behavioral deficits in animal models with schizophrenia-like behaviors during adolescence. *Molecular Psychiatry* **26**:2533-2552 https://doi.org/10.1038/s41380-020-01005-w | PubMed

29. **Iemi L,** Gwilliams L, Samaha J, Auksztulewicz R, Cycowicz YM, King JR, Nikulin VV, Thesen T, Doyle W, Devinsky O, *et al.* (2022) Ongoing neural oscillations influence behavior and sensory representations by suppressing neuronal excitability. *Neuroimage* **247**:118746 https://doi.org/10.1016/j.neuroimage.2021.118746 | PubMed

30. **Karmakar S,** Sarkar S (2013) Orientation enhancement in early visual processing can explain time course of brightness contrast and White's illusion. *Biological Cybernetics* **107**:337-354 https://doi.org/10.1007/s00422-013-0553-7 | PubMed

31. **Kato HK,** Gillet SN, Peters AJ, Isaacson JS, Komiyama T (2013) Parvalbumin-expressing interneurons linearly control olfactory bulb output. *Neuron* **80**:1218-1231 https://doi.org/10.1016/j.neuron.2013.08.036 | PubMed

32. **Kay LM,** Laurent G (1999) Odor– and context-dependent modulation of mitral cell activity in behaving rats. *Nature neuroscience* **2**:1003-1009 https://doi.org/10.1038/14801 | PubMed

33. **Lagier S,** Carleton A, Lledo PM (2004) Interplay between local GABAergic interneurons and relay neurons generates gamma oscillations in the rat olfactory bulb. *The Journal of Neuroscience* **24**:4382-4392 https://doi.org/10.1523/JNEUROSCI.5570-03.2004 | PubMed

34. **Lepousez G,** Lledo PM (2013) Odor discrimination requires proper olfactory fast oscillations in awake mice. *Neuron* **80**:1010-1024 https://doi.org/10.1016/j.neuron.2013.07.025 | PubMed

35. **Li WL,** Chu MW, Wu A, Suzuki Y, Imayoshi I, Komiyama T (2018) Adult-born neurons facilitate olfactory bulb pattern separation during task engagement. *eLife* **7** https://doi.org/10.7554/eLife.33006 | PubMed

36. **Lin TW,** Tan Z, Barik A, Yin DM, Brudvik E, Wang H, Xiong WC, Mei L (2018) Regulation of synapse development by vgat deletion from ErbB4-positive interneurons. *The Journal of Neuroscience* **38**:2533-2550 https://doi.org/10.1523/JNEUROSCI.0669-17.2018 | PubMed

37. **Lyons-Warren AM,** Tantry EK, Moss EH, Kochukov MY, Belfort BDW, Ortiz-Guzman J, Freyberg Z, Arenkiel BR (2023) Co-transmitting interneurons in the mouse olfactory bulb regulate olfactory detection and discrimination. *Cell reports* **42**:113471 https://doi.org/10.1016/j.celrep.2023.113471 | PubMed

38. **MacLeod K,** Laurent G (1996) Distinct mechanisms for synchronization and temporal patterning of odor-encoding neural assemblies. *Science* **274**:976-979 https://doi.org/10.1126/science.274.5289.976 | PubMed

39. **Margrie TW,** Sakmann B, Urban NN (2001) Action potential propagation in mitral cell lateral dendrites is decremental and controls recurrent and lateral inhibition in the mammalian olfactory bulb. *PNAS* **98**:319-324 https://doi.org/10.1073/pnas.011523098 | PubMed

40. **Matsuno T,** Kiyokage E, Toida K (2017) Synaptic distribution of individually labeled mitral cells in the external plexiform layer of the mouse olfactory bulb. *The Journal of Comparative Neurology* **525**:1633-1648 https://doi.org/10.1002/cne.24148 | PubMed

41. **Mei L,** Nave KA (2014) Neuregulin-ERBB signaling in the nervous system and neuropsychiatric diseases. *Neuron* **83**:27-49 https://doi.org/10.1016/j.neuron.2014.06.007 | PubMed

42. **Miyamichi K,** Shlomai-Fuchs Y, Shu M, Weissbourd BC, Luo L, Mizrahi A (2013) Dissecting local circuits: parvalbumin interneurons underlie broad feedback control of olfactory bulb output. *Neuron* **80**:1232-1245 https://doi.org/10.1016/j.neuron.2013.08.027 | PubMed

43. **Mohamed AAM,** Retzke T, Das Chakraborty S, Fabian B, Hansson BS, Knaden M, Sachse S (2019) Odor mixtures of opposing valence unveil inter-glomerular crosstalk in the Drosophila antennal lobe. *Nature Communications* **10**:1201 https://doi.org/10.1038/s41467-019-09069-1 | PubMed

44. **Moy SS,** Ghashghaei HT, Nonneman RJ, Weimer JM, Yokota Y, Lee D, Lai C, Threadgill DW, Anton ES (2009) Deficient NRG1-ERBB signaling alters social approach: relevance to genetic mouse models of schizophrenia. *Journal of Neurodevelopmental Disorders* **1**:302-312 https://doi.org/10.1007/s11689-009-9017-8 | PubMed

45. **Neddens J,** Fish KN, Tricoire L, Vullhorst D, Shamir A, Chung W, Lewis DA, McBain CJ, Buonanno A (2011) Conserved interneuron-specific Erbb4 expression in frontal cortex of rodents, monkeys, and humans: implications for schizophrenia. *Biological Psychiatry* **70**:636-645 https://doi.org/10.1016/j.biopsych.2011.04.016 | PubMed

46. **Nicolis di Robilant V,** Scardigli R, Strimpakos G, Tirone F, Middei S, Scopa C, De Bardi M, Battistini L, Saraulli D, Farioli Vecchioli S (2019) Running-activated neural stem cells enhance subventricular neurogenesis and improve olfactory behavior in p21 knockout mice. *Molecular Neurobiology* https://doi.org/10.1007/s12035-019-1590-6 | PubMed

47. **Nunes D,** Kuner T (2015) Disinhibition of olfactory bulb granule cells accelerates odour discrimination in mice. *Nature Communications* **6**:8950 https://doi.org/10.1038/ncomms9950 | PubMed

48. **Pardasani M,** Ramakrishnan AM, Mahajan S, Kantroo M, McGowan E, Das S, Srikanth P, Pandey S, Abraham NM (2023) Perceptual learning deficits mediated by somatostatin releasing inhibitory interneurons of olfactory bulb in an early life stress mouse model. *Molecular Psychiatry* **28**:4693-4706 https://doi.org/10.1038/s41380-023-02244-3 | PubMed

49. **Shi L,** Bergson CM (2020) Neuregulin 1: an intriguing therapeutic target for neurodevelopmental disorders. *Translational Psychiatry* **10**:190 https://doi.org/10.1038/s41398-020-00868-5 | PubMed

50. **Sohal VS,** Zhang F, Yizhar O, Deisseroth K (2009) Parvalbumin neurons and gamma rhythms enhance cortical circuit performance. *Nature* **459**:698-702 https://doi.org/10.1038/nature07991 | PubMed

51. **Sohrabi HR,** Bates KA, Weinborn MG, Johnston AN, Bahramian A, Taddei K, Laws SM, Rodrigues M, Morici M, Howard M, *et al.* (2012) Olfactory discrimination predicts cognitive decline among community-dwelling older adults. *Translational Psychiatry* **2**:e118 https://doi.org/10.1038/tp.2012.43 | PubMed

52. **Stakic J,** Suchanek JM, Ziegler GP, Griff ER (2011) The source of spontaneous activity in the main olfactory bulb of the rat. *PloS One* **6**:e23990 https://doi.org/10.1371/journal.pone.0023990 | PubMed

53. **Swaminathan S,** Shen L, Kim S, Inlow M, West JD, Faber KM, Foroud T, Mayeux R, Saykin AJ, Alzheimer's Disease Neuroimaging Initiative, *et al.* (2012) Analysis of copy number variation in Alzheimer's disease: the NIA-LOAD/NCRAD Family Study. *Current Alzheimer Research* **9**:801-814 https://doi.org/10.2174/156720512802455331 | PubMed

54. **Takahashi H,** Ogawa Y, Yoshihara S, Asahina R, Kinoshita M, Kitano T, Kitsuki M, Tatsumi K, Okuda M, Tatsumi K, *et al.* (2016) A subtype of olfactory bulb interneurons is required for odor detection and discrimination behaviors. *The Journal of Neuroscience* **36**:8210-8227 https://doi.org/10.1523/JNEUROSCI.2783-15.2016 | PubMed

55. **Tan Z,** Liu Z, Liu Y, Liu F, Robinson H, Lin TW, Xiong WC, Mei L (2022) An Erbb4-positive neuronal network in the olfactory bulb for olfaction. *The Journal of Neuroscience* **42**:6518-6535 https://doi.org/10.1523/JNEUROSCI.0131-22.2022 | PubMed

56. **Uchida S,** Shimada C, Sakuma N, Kagitani F, Kan A, Awata S (2020) The relationship between olfaction and cognitive function in the elderly. *The Journal of Physiological Sciences: JPS* **70**:48 https://doi.org/10.1186/s12576-020-00777-8 | PubMed

57. **Vullhorst D,** Neddens J, Karavanova I, Tricoire L, Petralia RS, McBain CJ, Buonanno A (2009) Selective expression of ErbB4 in interneurons, but not pyramidal cells, of the rodent hippocampus. *The Journal of Neuroscience* **29**:12255-12264 https://doi.org/10.1523/JNEUROSCI.2454-09.2009 | PubMed

58. **Walker IM,** Fullard ME, Morley JF, Duda JE (2021) Olfaction as an early marker of Parkinson's disease and Alzheimer's disease. *Handbook of Clinical Neurology* **182**:317-329 https://doi.org/10.1016/B978-0-12-819973-2.00030-7 | PubMed

59. **Wang CY,** Trotter JH, Liakath-Ali K, Lee SJ, Liu X, Sudhof TC (2021) Molecular self-avoidance in synaptic neurexin complexes. *Science Advances* **7**:eabk1924 https://doi.org/10.1126/sciadv.abk1924 | PubMed

60. **Wen L,** Lu YS, Zhu XH, Li XM, Woo RS, Chen YJ, Yin DM, Lai C, Terry AV, Vazdarjanova A, *et al.* (2010) Neuregulin 1 regulates pyramidal neuron activity via ErbB4 in parvalbumin-positive interneurons. *PNAS* **107**:1211-1216 https://doi.org/10.1073/pnas.0910302107 | PubMed

61. **Whitesell JD,** Sorensen KA, Jarvie BC, Hentges ST, Schoppa NE (2013) Interglomerular lateral inhibition targeted on external tufted cells in the olfactory bulb. *The Journal of Neuroscience* **33**:1552-1563 https://doi.org/10.1523/JNEUROSCI.3410-12.2013 | PubMed

62. **Xu Y,** Wang ML, Tao H, Geng C, Guo F, Hu B, Wang R, Hou XY (2022) ErbB4 in parvalbumin-positive interneurons mediates proactive interference in olfactory associative reversal learning. *Neuropsychopharmacology* **47**:1292-1303 https://doi.org/10.1038/s41386-021-01205-0 | PubMed

63. **Yoshitake M,** Maeshima E, Maeshima S, Sasaki K, Osawa A (2022) Association between cognitive function and olfactory identification ability in community-dwelling older individuals. *Journal of Physical Therapy Science* **34**:459-462 https://doi.org/10.1589/jpts.34.459 | PubMed

64. **Zavitz D,** Youngstrom IA, Borisyuk A, Wachowiak M (2020) Effect of interglomerular inhibitory networks on olfactory bulb odor representations. *The Journal of Neuroscience* **40**:5954-5969 https://doi.org/10.1523/JNEUROSCI.0233-20.2020 | PubMed

Peer reviews

Reviewer #1 (Public review):

Summary:

The authors have addressed many of the concerns. In sum, this study examined how ErbB4 signalling in parvalbumin-positive (PV) interneurons contributes to olfactory bulb (OB) microcircuit function and olfactory behaviour in mice. Using RNAscope, single-cell RT-PCR, conditional Erbb4 deletion, awake in vivo recordings, slice electrophysiology and optogenetics, the authors report that ErbB4 was expressed in PV interneurons of the EPL and IPL, and that its loss impaired odour discrimination and dishabituation, reduced GABAergic transmission onto mitral cells, and elevated ongoing LFP power. The experiments were well-designed, but several central claims were not yet adequately supported by the data as presented.

Strengths:

Pretty comprehensive set of experiments.

Weaknesses:

(1) Figure 1. The investigation time of the AAV-Cre-GFP group varied considerably across isoamyl acetate concentrations. Were there any differences between the AAV-GFP and AAV-Cre-GFP groups at the 0 (mineral oil) condition? Since the threshold was defined by a

comparison against mineral oil, a baseline difference would propagate directly into the threshold estimate and could reduce exploratory drive rather than an olfactory deficit.

(2) Previous papers have reported that ErbB4 is expressed in neuroblasts of the SVZ and RMS, and that disruption of NRG1-ErbB4 signalling may decrease GABAergic neuron number and alter distribution (Anton et al., Nat Neurosci 2004; Ghashghaei et al., PNAS 2006). The authors showed in Figure 2L that ErbB4 expression in the OB was already decreased at P7, suggesting reduced neuron number and disrupted neuronal distribution. The authors should therefore quantify the number and laminar distribution of the different neuronal types in the OB. Cresyl violet staining showed that gross lamination was preserved, but could detect changes in cell density or in the relative proportions of interneuron subtypes.

(3) Figure 4C. First of all, there were no indicators marking the sessions, so we had no idea what state the mice were in. Also, why did the odour-evoked MFRs of PV-Erbb4$^{+/+}$ and PV-Erbb4$^{-/-}$ mice show opposite trends during the 0-2 s window in the first session - were there any differences in the behaviour of the two groups during this session? As the mice were head-fixed on a floating ball, locomotion and sniffing should have been monitored, since both strongly influence M/TC firing.

(4) Figure 4K-L. The authors did not explain why spontaneous and odour-evoked MFR were so much different among the "no response" M/TCs. Did this mean that ErbB4 knockout in PV interneurons disrupts the function? This would imply a tonic rather than a stimulus-locked disinhibition, which is a different claim from the one made in the Discussion. In addition, the authors stated that panel 4L indicates "the distribution of types of odour-evoked responses was significantly altered in PV-Erbb4$^{-/-}$ mice compared with PV-Erbb4$^{+/+}$ mice, suggesting compromised odour detection" - what exactly does this mean? A shift in the proportions of response categories is also compatible with a changed baseline firing rate altering the classification itself.

(5) Figure 5. The power of all frequency bands in PV-Erbb4$^{-/-}$ mice was higher than in PV-Erbb4$^{+/+}$ mice, including the gamma band. However, Tan et al. (2022) reported that inhibition of ErbB4 kinase activity decreases LFP power and GABA release, which is inconsistent with the present data. This discrepancy should be addressed explicitly. A uniform elevation across all four bands was atypical for a PV-dependent mechanism and could reflect a global scaling difference; separating periodic from aperiodic components and reporting normalised power would help.

(6) Photocurrent amplitude and mCherry^{+} PV cell density was not compared across genotypes; Figure 9-figure supplement 1B-C showed photocurrents for only one group. Since the authors themselves reported in Figure 7-figure supplement 1 that PV interneurons in knockout mice reduced mEPSC frequency and amplitude and increased AP frequency, the presynaptic population was clearly not in an equivalent state. The reduced oIPSC could therefore result from differences in ChR2 expression level or in the number of labelled cells. Photocurrent curves and mCherry^{+} cell density must be provided for both groups.

https://doi.org/10.7554/eLife.101237.2.sa2

Reviewer #2 (Public review):

The authors aimed to understand how the transcription factor Erbb4 contributes local circuit dynamics and affects performance. This is an interesting question because Erbb4 is largely localized to PV cells in the olfactory bulb (OB) and upregulated following exposure to an olfactory discrimination task.

Strengths:

They have now validated their local, PV-specific knockout strategy, which more directly tests their hypothesis.

The inclusion of optogenetically evoked presynaptic responses from PV cells onto M/T cells also strengthened the conclusion that this synapse was altered.

The authors also now included slice recordings from PV cells, which helps to form a more comprehensive picture of the circuit.

Weaknesses:

(1) The data used to support their spike sorting approach is now included but is difficult to evaluate. In Figure 4 - supp 1B, they show what appears to be mean + sem of concatenated waveforms from one tetrode, but this is not explained anywhere. Moreover, the timescale seems to be off by an order of magnitude. It also seems that the spike widths in panel E are bimodally distributed, with many of the half-widths being more consistent with fast-spiking cells. There is a high density of PV cells in the same layer where they record M/T cells, so is it not possible that some of the units were PV cells (note: this was suggested in the previous review as a potential exciting direction to further validate their findings)? It is still unclear how the authors confidently record from only M/T cells when there is no mention of how other units (e.g., fast-spiking cells) are excluded. The methods state that only M/T cells can be recorded from this layer, which is an oversimplification and appears at odds with the apparent diversity in waveforms and responses.

(2) Upon review, the authors acknowledge that the PV-Erbb4+/+ and PV-Erbb4-/- mice were recorded in separate batches where the control mice were exposed to unwanted artefacts related to a solenoid valve. While we don't know how much that change influenced the results, even with careful analysis, it does draw attention to a major weakness in study design where controls and experimental mice are not run simultaneously. The presence of an artefact from the solenoid valve (perhaps a noise?) immediately before odor presentation for controls, but not experimental mice, should be considered by the reader when it comes to evaluating the odor-evoked responses.

Overall, I feel the manuscript is much improved and more solidly demonstrates that Erbb4 expression in PV cells plays a major role in regulating local OB circuit dynamics and influences odor processing. The remaining weaknesses surrounding the in vivo single unit recordings from PV-Erbb4+/+ versus PV-Erbb4-/- mice reduce my confidence in the validity of the results, but the general agreement of the in vitro work is more re-assuring.

https://doi.org/10.7554/eLife.101237.2.sa1

Author response:

The following is the authors' response to the original reviews.

> ***Public Reviews:***
>
> ***Reviewer #1 (Public review):***
>
> *Summary:*
>
> *The study by Hu et al. investigated the role of olfactory ErbB4 in regulating olfactory information processing. The authors demonstrated that ErbB4 deletion impairs odor discrimination, sensitivity, habituation, and dishabituation by using an impressive combination of techniques from morphological to electrophysiology (both slice and in vivo) and from viral injection to cell-type-specific mutation to behavioral analysis. The*

> *findings underscore the crucial role of ErbB4 in olfactory PV neurons in modulating mitral cell function and odor perception.*
>
> *Strengths:*
>
> *This study contains a pretty comprehensive set of experiments.*
>
> *Major concerns:*
>
> *(1) Line 151 page 7, "PV-Erbb4+/+ mice (generated by crossing PV-Cre mice (Wen et al., 2010) with loxP-flanked Erbb4 mice". Does this mean mice carrying PV-Cre and ErbB4 floxed allele? Or with the WT allele? This is confusing. Figures 2B and 2C, ErbB4 expression was evident in many cells that were not positive for PV. What are the identities of those cells? Are they important?*

Thank you for your positive comments regarding our study. PV-*Erbb4*$^{+/+}$ mice carried the PV-Cre transgene with the WT allele. In the revised manuscript, we have simplified the description of the genotype for clarity and have provided detailed breeding information in the "Materials and Methods" section (Line 532).

As shown in Figures 2B and 2C, ErbB4 expression was evident in GL and GCL cells that were not positive for PV. The activation of ErbB4-expressing cells in the GL and GCL has been suggested to upregulate theta and gamma oscillations, respectively (PMID:35853717). Mammalian OB are the most abundant and varied interneurons among brain tissues, and their functional importance and diversity remain unclear (PMID:31358754 and PMID:32208366). ErbB4-expressing PV interneurons in the EPL and IPL were relatively less abundant but accounted for the majority of inhibitory inputs to M/TCs. Importantly, one PV interneuron connects with over 1000 M/TCs to mediate recurrent and lateral inhibition, linearly controlling the OB output (PMID:31358754 and PMID:39186804). This study provides evidence that ErbB4 signalling in PV interneurons is required for olfactory discrimination and dishabituation.

> *(2) In Figure 4, the authors performed tetrode recordings in awake head-fixed animals. Although individual neuron spikes could be obtained by spike-sorting, this is not a "single-unit" experiment due to the nature of this approach.*
>
> *What is the odor used in Figure 4? How did the authors clean up the odor to limit the stimulation within 2 seconds? In what layer were the tetrodes placed? What is the putative cell type presented in Figure 4C? If Figure 4C is a representative neuron recorded, the odor-induced suppression of spike activity seems to be impaired in PV-ErbB4-/- animals. However, Figure 4D shows that suppressed neurons were similar between the two types of animals. Such comparisons among individual mice are difficult for in vivo electrophysiological experiments because the recorded cell type and placement of electrodes would be different. The authors should apply ErbB4 inhibitors to the same animals and compare the effects before and after. This would ensure the recording of the same population of neurons.*

Thank you for your valuable comment and suggestion. We agree that tetrode recording combined with spike-sorting is not a strict "single-unit" approach, although this method is widely accepted and consistently referred to as "single-unit recording" even "single-neuron recording" (PMID:30833706). Based on your comments, we modified the description as follows: “To obtain individual neuron spikes, units were identified by principal-component analysis scan (PCA) clustering of the spikes” (Lines 210-212).

As shown in Figure 4, a standardised panel with eight tubes delivers eight odours: isoamyl acetate, 2-heptanone, phenyl acetate, benzaldehyde, dimethylbutyric acid, n-heptanoic acid, n-pentanol, and 2-pentanone. Odours were delivered via an odour delivery system

(Thinkerbiotech), and charcoal-filtered air was supplied to the mouse's nose at a constant rate of 1 L/min to eliminate airflow interference, which effectively limited the stimulation to 2s. We have added the above description to the revised "Materials and Methods" section (Lines 786-789).



Author response image 1.

The tetrodes were placed within the ventral mitral cell layer based on stereotaxic coordinates. The putative cell type is mitral/tufted (Figure 4C). Despite the presence of diverse cell types in the OB, only the spiking activity of M/TCs can be captured via tetrode recordings (Kay and Laurent, 1999; Doucette et al., 2011). We added the above description in the revised "Materials and Methods" section (Lines 764-767). As you have indicated, Figure 4C shows the impairment of odour-induced spike suppression in PV-*Erbb4*$^{-/-}$ mice. Consistently, Figure 4D shows the decreased suppression of odour-induced spike activity in blue (quantified in Figure 4I ΔMFR, ~25%), but the increased number of suppressed neurones in the PV-*Erbb4*$^{-/-}$ group (Figure 4L). Considering that applying ErbB4 inhibitors to the same animals has no selectivity for blocking ErbB4 signalling in PV interneurons, *in vivo* neural signals typically drift over time when performing pre- and post-inhibition comparisons. Therefore, we compared *in vivo* electrophysiological data at the population level according to previous studies (PMID: 35173173, PMID:28425486, and PMID:28817803).

> *(3) At a glance in the heatmap in Figure 4D, excited neurons were reduced in PV-ErbB4-/- mice, but not inhibited neurons. This was different from Figure 4L. The authors need to have a criteria or threshold to show how they categorized each population.*

In Figure 4L, red denotes excited neurones, whose number decreased from 66 to 16 in the PV-*Erbb4*$^{-/-}$ group, and blue denotes inhibitory neurones, whose number increased from 81 to 148 in the PV-*Erbb4*$^{-/-}$ group. This trend is consistent with that observed in Figure 4D. The classification criteria for each population were defined as follows:

"To determine whether the odour evoked a significant response, we used the Wilcoxon signed-rank test to compare the spontaneous (baseline) firing rate and odour-evoked firing rate of each unit–odour pair across all trials; unit–odour pairs with $P > 0.05$ were defined as nonresponsive, those with $P < 0.05$ as responsive, and responsive pairs were further categorised as excitatory (odour-evoked firing rate > spontaneous firing rate) or inhibitory (odour-evoked firing rate < spontaneous firing rate). Details are provided in the "Off-line spike sorting and statistics of the unit data" section of Materials and Methods (Lines 810-816).

> *(4) Figure 4D, 4F and 4J seemed to be inconsistent. In Figure 4D before odor, there was no clear increase in the spontaneous activity in PV-ErbB4-/- mice; in Figure 4F-4G and 4J-4K, clearly, there was a high spontaneous activity in PV-ErbB4-/- mice.*

Figure 4D, 4F and 4H shows odour-evoked changes in mean firing rate (ΔMFR), calculated by subtracting the baseline firing rate. By contrast, Figures 4G and 4I show raw spontaneous mean firing rate (MFR), which was elevated in PV-*Erbb4*$^{-/-}$ mice. We have revised the description of Figure 4D in both the Results section (Line 222) and figure legends (Line 1217).

> *(5) What are the neurons recorded in Figure 6E-6F? If they were MCs, loss of ErbB4 in PV neurons should not alter their intrinsic electrical properties. Rather GABAergic inputs could be altered. Indeed, the authors presented a reduction of GABAergic inputs from PV neurons to MCs.*

The neurones recorded in Figures 6E-6F are indeed mitral cells (MCs). The firing frequency of action potentials reflects not only the intrinsic electrical properties but also the balance between excitatory and inhibitory synaptic inputs. As demonstrated in this study, the loss of ErbB4 in PV neurones leads to reduced GABAergic synaptic inputs from PV interneurons to MCs, which is consistent with our reasoning and is a key factor contributing to the observed changes in the action potential firing of MCs

> *(6) Figure 8E-8H, a better experiment would be specifically expressing ErbB4 or PV neurons. In Figure 8F and Figure 8I, was it the excitability after the current injection? Why not perform the spontaneous activity recording?*

According to your suggestion, we used optogenetics to activate PV interneurons and recorded inhibitory postsynaptic currents (IPSCs) in MCs. As shown in the revised Figure 9 and Supplementary Figure 1F and 1G, deleting ErbB4 of PV interneurons in the OB weakened the inhibitory modulation of MCs by PV interneurons.

Figures 8F and 8I show the excitability after current injection. We did not measure spontaneous activity, primarily because the spontaneous firing frequency varies significantly among different cells, resulting in poor stability. In contrast, current-injection-induced excitability is more stable and quantifiable, making it more suitable for assessing specific changes in MC responsiveness caused by altered PV-MC inhibitory inputs.

> ***Reviewer #2 (Public review):***
>
> *Summary:*
>
> *Hu et al investigate the role of PV neurons and their expression of Erbb4 in olfactory performance through a series of behavioral tests, selective knockout experiments, and in vivo and in vitro electrophysiology. Knockout of Erbb4, either in PV cells or the whole OB, resulted in impairment of discriminating complex odors. The authors present data that inhibition is impaired in MCs, which is likely underlying the abnormal odor-evoked responses of MCs in vivo and the impaired behavioral responses.*
>
> *Strengths:*
>
> *Overall, a key strength of this manuscript is the breadth of experiments to test the role of PV Erbb4 expression on circuit dynamics and behavior. The behavioral experiments were clear and sufficiently powered.*
>
> *Weaknesses:*
>
> *The major drawback of this manuscript is the lack of depth and rigor in experiments. Some experiments are preliminary, underpowered, and not quantified. As a result, many conclusions of the manuscript are weakly supported in its current form and would require significant revisions to address these shortcomings. Major weaknesses that should be addressed are as follows:*

> *(1) AAV-PV-Cre-GFP is not described or validated. Is this the S5E2 enhancer or something else? What is the specificity and efficacy of this approach in selectively knocking out Erbb4 in PV neurons? Reduced Erbb4 expression in the entire OB with PCR does not validate the selectivity of this approach. At a titer of 10^12, it is unlikely to be specific. Even a small amount of off-target Cre expression will knock out the gene in non-PV cells, so the authors should show whether the gene is knocked out at the single-cell level from PV and non-PC cells. Without validation of this approach, this experiment is no different than the AAV-Cre-GFP experiments.*

Thank you for your comment and thoughtful suggestion. The AAV-PV-Cre vector used in this study was purchased from BrainVTA (catalogue number: PT-0275; vector name: rAAV-fPV-CRE-bGH polyA), which contains an fPV promoter to ensure the selectivity and a β-globin intron to enhance Cre expression efficiency. Importantly, the specificity and efficacy of this AAV-PV-Cre construct in selectively targeting PV-expressing neurones have been validated in multiple published studies (PMID:40196908 and PMID:31987494). According to your suggestions, we also performed immunofluorescence staining (co-staining for PV and ErbB4) and found that ErbB4 expression was specifically reduced in PV-positive interneurons in OB tissues injected with AAV-PV-Cre, while ErbB4 levels remained unchanged in PV-negative cells (the revised Figures 9B and 9C). This single-cell-level validation directly demonstrated that our AAV-PV-Cre-mediated knockout approach specifically targets ErbB4 in OB PV interneurons, thereby avoiding off-target effects in non-PV cells.

> *(2) Figure 1D - three mice per group is insufficient. There is no control group error (the same as Figure 9). Why is it a paired t-test when there is a control group? The authors should be comparing go/go vs. go/no-go. The methods for normalization are unclear and are likely to hide the fact that n=3 is insufficient to capture a difference without extra measures to normalize the data.*

Thank you for the comment. According to your suggestions, we expanded the sample size to four mice per group and modified the statistical test from a paired *t*-test to an unpaired *t*-test in the revised Figure 1C and 1D. Since not all samples were exposed to the same blot for direct comparison, we performed normalisation of each sample relative to its internal control prior to statistical analysis to ensure the reliability of group comparisons. There was an error regarding the control group in the revised Figure 1D. Detailed information on the normalisation method and updated statistical results have been provided in the revised figure legends (Lines 1116-1118).

> *(3) The analysis of LFP is limited. During what period was this quantified? Are there any differences in task-related LFP changes? Also related to in vivo electrophysiology, the authors should show examples of isolated units, including their waveforms and how units were clustered and assigned to M/TCs.*

Thank you for the comment. The spectral power of each frequency band was quantified using a 4-s sliding window during the pre-odour stimulation period (4–0 s before odour onset). Regarding task-related LFP changes, the initial recordings were affected by unavoidable interference, leading to unstable signals that precluded reliable analyses. Based on your suggestions, we have supplemented the revised manuscript with examples of isolated single units, including their representative waveforms, clustering results (e.g. principal component analysis plots), and unit assignment criteria (the revised Figure 4—figures supplement 1A and 1B). As previously noted, the tetrodes were placed in the mitral cell layer based on stereotaxic coordinates. Consistent with established literature (Kay and Laurent, 1999; Doucette et al., 2011), the putative cell type recorded using this approach was mitral/tufted cells (M/TCs). Detailed methodological parameters for spike sorting, unit isolation, and cell type identification are provided in the "Materials and Methods" section (Lines 764-767 and Lines 803-805).

> *(4) The authors use 80pA and 100pA to elicit equivalent AP spiking in MCs to determine if recurrent inhibition differs, but do not actually show that AP spiking is the same across groups. This should be quantified.*
>
> *There seems to be a prominent increase in the firing of MCs in PV-Erbb4+/+ mice before odor presentation, but not in PV-Erbb4-/- mice. What is the significance of this?*

Thank you for your valuable comment and suggestion. According to your suggestions, we quantified the AP firing frequency of MCs in both groups under the respective stimulation currents, and statistical analysis confirmed that there was no significant difference in the AP spiking levels between the two groups (the revised Figure 8—figure supplement 1A).

We speculate this prominent pre-odour firing increase in PV-*Erbb4*$^{+/+}$ mice (but not in PV-*Erbb4*$^{-/-}$ mice) stems from interference caused by the opening of the solenoid valve during odour clearance prior to stimulation—this artefact was present in the initial recordings of control mice but was eliminated during the data acquisition for PV-*Erbb4*$^{-/-}$ mice. This was not statistically significant. To avoid this interference, we strictly defined the analysis windows, and the spontaneous firing rate was calculated by averaging the spikes recorded during the 4–2 s period before odour stimulation, excluding the interference-prone interval immediately before odour onset. This rigorous window selection ensured the reliability of our comparisons of spontaneous and odour-evoked firing between the groups.

> *(5)There is a disconnect between the in vivo firing rates of MCs and ex vivo firing rates. In slice, the authors note that the spontaneous activity of MCs is elevated in the KO, but this is not observed in vivo, where conditions are physiological. Therefore, it is unclear whether the concept of signal-to-noise changes in slice (higher spontaneous, lower evoked), indeed translate to something in vivo. It would be important to know what the PV cells are doing in vivo. Perhaps they have low firing rates prior to odor onset, which may explain the lack of observed difference in baseline FRs in MCs. The authors should have this data in their tetrode recordings, which would offer insight into when inhibition is recruited.*

Thank you for your valuable comments, which helped clarify the consistency between *in vivo* and *ex vivo* electrophysiological data. In *ex vivo* slice recordings, we measured both spontaneous and evoked excitatory firing rates of MCs, and found that the spontaneous activity of MCs was elevated in PV-*Erbb4*$^{-/-}$ mice (Figures 6A and 6B). Importantly, this observation is consistent with our *in vivo* data: M/TCs in PV-*Erbb4*$^{-/-}$ mice exhibited significantly higher spontaneous firing rates during excitatory responses to odour presentation (Figures 4F and 4G). However, for inhibitory responses during odour presentation, M/TCs in PV-*Erbb4*$^{-/-}$ mice showed significantly lower spontaneous firing rates *in vivo* (Figures 4H and 4I). Thus, the overall *in vivo* spontaneous activity of MCs appeared unchanged owing to opposing changes in excitatory and inhibitory subpopulations, and there was no true discrepancy between the *ex vivo* and *in vivo* results. We agree that *in vivo* recording of PV interneuron activity would be invaluable for understanding their functional state under physiological conditions. Unfortunately, this is technically unfeasible with the current experimental setup, primarily because of the sparse distribution of PV interneurons in the OB. As a complementary alternative, we characterised the key electrophysiological properties of PV interneurons in *ex vivo* slices (e.g. action potential and mEPSC, the revised Figure 7—figure supplement 1), which will provide additional insights into the underlying cellular mechanisms.

> *(6) Since PV neurons are required for gamma oscillations, why is it that KOs have higher gamma oscillations? Is it indeed the case that PV cells have a hypofunctional phenotype in this model? Again, recording from PV cells in vivo would help make sense of this.*

Thank you for your valuable comments, which were critical for clarifying the functional consequences of ErbB4 knockout in PV interneurons. The elevated gamma oscillations in the OB of PV-*Erbb4*$^{-/-}$ mice appear to be primarily driven by the increased action potential firing frequency of PV interneurons that we observed in OB slice recordings (the revised Figure 7—figure supplement 1). A similar phenomenon has been reported in the hippocampus (PMID:24050403).

Indeed, the PV cells displayed a hypofunctional phenotype in this model. Our optogenetic experiments provided direct evidence for this (the revised Figure 9—figure supplement 1). Specifically, optogenetic activation of PV interneurons in AAV-PV-Cre-injected mice (selective ErbB4 knockout in OB PV interneurons) induced weaker inhibitory postsynaptic currents (IPSCs) in MCs than in controls (the revised Figure 9—figure supplement 1). This indicates that ErbB4 loss induces PV interneurons to be more excitable, but impairs their ability to inhibit neighbouring MCs.

We acknowledge that *in vivo* recordings of PV interneurons would further clarify their functional state under physiological conditions. As noted earlier, this remains technically challenging using our current setup; however, our *ex vivo* mechanistic data and optogenetic findings collectively support these conclusions.

> *(7) A clearer picture of how PV cell inhibition changes with Erbb4 KO would be achieved with optogenetically evoked IPSPs, rather than changes in mini frequency.*

Thank you for the comment. Based on your suggestions, we used optogenetics to activate PV interneurons and recorded the optogenetically evoked inhibitory postsynaptic currents (oIPSCs) in MCs. As shown in the revised Figure 9 and Supplementary Figure 1F and 1G, deleting ErbB4 in PV interneurons in the OB weakened the inhibitory modulation of MCs by PV interneurons.

> ***Reviewer #3 (Public review):***
>
> *Summary:*
>
> *The authors investigate the role of ErbB4 in parvalbumin (PV) interneurons within the olfactory bulb (OB) and its regulation of odor discrimination behavior in mice. They demonstrate that odor discrimination increases ErbB4 kinase activity and that the loss of ErbB4 in the OB impairs the dishabituation of odor response and discrimination of complex odors. The study also characterizes the expression of ErbB4 in the OB, showing it is enriched in PV neurons. Furthermore, the authors utilize a mouse model in which ErbB4 is knocked out in PV neurons and perform a variety of behavioral, electrophysiological, and local field potential (LFP) recording experiments to characterize alterations in olfactory bulb activity. They then use a model in which ErbB4 is specifically knocked out in PV neurons in the OB and show that this manipulation disrupts odor-related behaviors in mice.*
>
> *Strengths:*
>
> *The study's strengths lie in its use of a diverse range of techniques, including RNAscope, IHC, and Western blotting, to assess the presence of ErbB4 in PV neurons within the OB. Additionally, the authors employ various behavioral tests to evaluate the effects of ErbB4 manipulation in different mouse models, alongside comprehensive electrophysiological experiments and LFP recordings to examine the impact of these manipulations on OB physiology.*
>
> *Weaknesses:*

> *While the data presented in this paper are interesting, several major concerns reduce my enthusiasm for this study, as outlined below:*
>
> *(1) In reviewing Figure 1C/D, there are several concerns regarding the clarity and interpretation of the data:*
>
> *(a) While the Western blot for ErbB4 in other figures (Figure 1F, 2I) of the manuscript shows a clear single band, the blot presented in Figure 1C (for both p-ErbB4 and total ErbB4) shows multiple bands, which is unexpected. This discrepancy raises concerns about the consistency of the results.*
>
> *(b) The data presented in Figure 1D uses only 3 mice per group, and the reported p-value of 0.0492, while technically significant, is very close to the threshold. This raises concerns about the robustness of the finding, especially given the small sample size. Additionally, the p-ErbB4 band intensity in the Go/No-Go condition in Figure 1C does not appear to show a clear increase over the Go/Go condition, which is not congruent with the bar graph in Figure 1D showing a 50% increase in p-ErbB4/ErbB4 levels.*
>
> *(c) It is a standard practice in many journals to include full, uncropped Western blot images as supplementary material. This transparency helps ensure that no bands are selectively shown or omitted and increases confidence in the presented data.*

Thank you for your comment and thoughtful suggestion.

(a) The multiple bands observed for both p-ErbB4 and total ErbB4 in the original Figure 1C are likely attributable to the high concentration of the primary antibody used initially (Santa Cruz Biotechnology), which has since been discontinued. In the revised manuscript, we have replaced the original antibody with an anti-ErbB4 antibody (Cat# 4795, Cell Signalling Technology), which showed a single ErbB4 band (the revised Figure 1C). To detect p-ErbB4, we first performed immunoprecipitation with a phosphorylated tyrosine antibody to enrich the total phosphorylated proteins, followed by immunoblotting for ErbB4.

(b) According to your comments, we have expanded the sample size to four mice per group and modified the statistical test to an unpaired *t*-test in the revised Figure 1D.

(c) We included all relevant uncropped blot images in the Supplementary Material (the revised Figure 1, 2—figure supplement 1).

> *(2) In Figure 2, the authors used the anti-ErbB4 antibody sc-283 from Santa Cruz to assess the expression of ErbB4 in PV neurons and the absence of its expression in PV-ErbB4 knock-out mice. However, this particular antibody has been shown to produce non-specific bands in Western blotting and also generate non-specific labeling in IHC. This non-specificity has been demonstrated in Vullhorst et al. (2009, J Neurosci), raising significant concerns about the reliability of the data generated using this antibody.*

Thank you for the comment. As you have indicated, the non-specificity of the anti-ErbB4 antibody sc-283 has been reported in J Neurosci (Vullhorst et al, 2009). These antibodies have been widely used in numerous recent studies (PMID:39543371 and PMID:41297670), indicating their utility for assessing ErbB4 expression under appropriate experimental conditions (primary antibody dilution and incubation conditions). As shown in the revised Figure 2I and 2J, the absence of ErbB4 expression in PV-ErbB4 knock-out mice proved the specificity of the antibody for immunofluorescence staining. To address these potential concerns, we conducted a rigorous validation tailored to our model. In the revised manuscript, we complemented the protein-level detection with RT-PCR, which directly validated the specific knockout of *Erbb4* mRNA in PV neurones (the revised Figure 2F-H). Additionally, we performed follow-up immunofluorescence staining experiments using a

well-validated anti-ErbB4 antibody (19943-1-AP, Proteintech; see PMID: 37060105) to assess the expression of ErbB4 in PV neurones (the revised Figure 9B and 9C).

> *(3) In reviewing the statistical analysis for the series of odor discrimination tests, there could be a potential issue with the clarity of the significance testing. Although the figure legend reports the F and p values from the two-way ANOVA, it is unclear whether these values represent the main effects or the results of a post hoc test. Additionally, it is not clear whether the asterisk in the figures reflects significance from a post hoc test or from the overall ANOVA. The methods section does not explicitly state whether a post hoc test was performed to assess differences between the knockout and control groups. Given that the tests were conducted across multiple days or conditions, a post hoc test that can adjust for multiple comparisons would be necessary to accurately identify where specific differences between the groups exist.*

Thank you for your comment and suggestion. For the odour discrimination tests, two-way ANOVA was followed by Tukey's post hoc adjustment for multiple pairwise comparisons, which is explicitly stated in the revised Methods section (Lines 832-833). According to your suggestions, we have revised the figure asterisks to indicate significant post hoc differences between the groups.

> *(4) Throughout the manuscript, the authors use different mouse models, including ErbB4 knockout specifically in the OB (AAV-Cre-GFP), ErbB4 knockout in PV interneurons throughout the brain (PV-ErbB4-/-), and ErbB4 knockout in PV interneurons within the OB (AAV-PV-Cre-GFP). For Figures 4 and 5, the authors use the PV-ErbB4-/- model to examine odor-evoked activity and neural oscillations within the OB. Since the knockout affects PV interneurons across the entire brain, it is difficult to disentangle whether the observed changes in the OB are due to local effects or broader network alterations elsewhere in the brain.*

Thank you for the comment. We first clarify the rationale for initially using the whole-brain PV-*Erbb4*$^{-/-}$ model: this model is well-validated and widely adopted in *in vivo* electrophysiological studies targeting brain region-specific phenomena, such as regulating synaptic plasticity in the hippocampus (PMID:24050403) and modulating sensory coding in the cortex (PMID: 37069344).

Additionally, PV interneurons in the OB are local-projection neurones that exert stronger and more extensive inhibitory effects on M/TCs, a key feature that restricts their functional impact primarily to the local OB circuit rather than broader cross-brain network interactions, further supporting the relevance of the global model for OB-focused research.

Furthermore, local AAV-Cre injections have notable experimental limitations in our electrophysiological recordings. Stereotaxic infusion induces mechanical trauma and local inflammation in the OB, altering basal circuit activity independent of ErbB4 deletion. AAV also yields incomplete mosaic gene ablation among PV interneurons, introducing a variable knockout efficiency that complicates the interpretation of local electrophysiological readouts. In comparison, the global PV-*Erbb4*$^{-/-}$ line mediates uniform, complete ErbB4 deletion across all PV interneurons, avoiding viral artefacts and rendering our OB electrophysiological measurements more reliable for assessing endogenous local circuit function.

> *(5) While the electrophysiological experiments shown in Figures 6-8 provide valuable insights into the reduced inhibition to MCs in PV-ErbB4 knockout mice, it appears that the authors did not record from PV interneurons themselves. Since PV interneurons are central to the proposed mechanism, directly recording them would provide critical information on how the ErbB4 knockout affects their intrinsic properties, synaptic inputs, and firing behavior. Without these direct recordings, the conclusions about the specific role of PV neurons in regulating MC activity remain somewhat indirect. Prior studies*

> *have established that knockout of ErbB4 in PV interneurons reduces mEPSC frequency in PV neurons (Del Pino et al., 2013).*

Thank you for your valuable comment and suggestion. According to your suggestions, we have supplemented the electrophysiological experiments (the revised Figure 7—figure supplement 1) with direct recordings from PV interneurons in *ex vivo* slices. These recordings revealed that ErbB4 knockout alters some properties of PV interneurons (e.g. action potential frequency), reduces mEPSC frequency (consistent with Del Pino et al., 2013), and modulates their firing behaviour, directly confirming that ErbB4 deletion affects PV interneurons.

> *(6) In Figure 9, the authors knock out ErbB4 in PV neurons in the OB with AAV-PV-Cre-GFP and show with western blotting that ErbB4 expression is reduced in the mouse injected with AAV-PV-Cre-GFP. However, it is not clear whether ErbB4 was selectively knocked out in PV neurons without the quantification from IHC assays.*

Thank you for the comment. To verify the selective knockout of ErbB4 in OB PV neurones, we performed an additional experiment: immunofluorescence co-staining for PV and ErbB4; quantitative analysis confirmed a significant reduction of ErbB4 in PV interneurons in AAV-PV-Cre–injected mice (the revised Figure 9B and 9C).

> ***Recommendations for the authors:***
>
> ***Reviewer #1 (Recommendations for the authors):***
>
> *Other concerns:*
>
> *(1) No supplemental Figure 1 was shown.*

We apologise for the oversight. Supplemental Figure have been included in the revised manuscript (the revised Figure 2—figure supplemental 2).

> *(2) In line 59, page 3, abbreviations of mitral/tufted cells (M/TCs) or "MCs" were confusing.*

We have clarified the abbreviation by explicitly defining "mitral cells (MCs)", with "M/TCs" retained for mitral/tufted cells to avoid ambiguity (Line 56-59).

> *(3) The quality of blots in Figure 1C was less satisfactory, with lots of noisy bands. Maybe antibodies from Cell Signaling should be used.*

We optimised the experiment as suggested. In the revised Figure 1C, we have used an anti-ErbB4 antibody (Cat# 4795, Cell Signalling Technology) combined with the immunoprecipitation-immunoblotting workflow.

> *(4) The authors should describe the serotype as well as the promoters of AAV-Cre-GFP used in the experiments.*

As you suggested, we have supplemented the details of AAV-Cre-GFP in the Methods section: Viruses driven by the CAG promoter, including pAOV-CAG-EGFP-T2A-Cre (catalogue No. CN396, serotype AAV2/8) and pAOV-CAG-EGFP-2A (catalogue No. CN394, serotype AAV2/8) were purchased from Obio Technology, Shanghai, China (Lines 568-571).

> *(5) The authors should describe the binary mixtures of isoamyl acetate Vs. Heptanone. Simply 6/4 Vs. 4/6 is not easy to follow.*

As you suggested, we have clarified the binary odour mixtures in the Results section: (60%/40% binary mixtures of these odours, "6/4" refers to 60% isoamyl acetate + 40% heptanone, and "4/6" refers to 40% isoamyl acetate + 60% heptanone, in volume) (Lines 111-113).

> *(6) Figure 1G, "0 limonene" AAV-Cre-GFP group did not show the error bar.*

We apologise for the omission—error bars for the "0 limonene" AAV-Cre-GFP group have been added to the revised Figure 1.

> *(7) Figure 2A, the green signal for ErbB4 was not that strong, it was hard to visualize the expression of ErbB4 in five layers of OB.*

Thank you for the comment. The revised Figure 2A shows an enhanced green signal for ErbB4, clearly indicating its distribution in all OB layers.

> *(8) The authors should clearly label or indicate the cell type of neurons recorded in Figure 6, Figure 7, and Figure 8A-8C.*

As you suggested, we have clearly labelled the cell types in the revised Figures 6, 7, and 8A–8C: all recorded neurones are mitral cells (MCs).

> *(9) line 320-321, page 14, "Figures 8F and 8G, a burst of conditioning 320 stimuli (40 pulses at 100 Hz)", the authors should indicate the stimuli as a tick or scale on Figures 8F and 8I.*

As per your suggestion, we have added scales and vertical ticks to the revised Figures 8F and 8I to indicate the timing of the conditioning stimuli (40 pulses at 100 Hz).

> ***Reviewer #2 (Recommendations for the authors):***
>
> *(1) Figure 1F is not quantified.*

As suggested, we have supplemented the quantitative analyses of Figure 1F (see the revised Figure 1G) and the statistical details in the revised legend.

> *(2) Figures 2G and H are not quantified.*

As suggested, we have supplemented the quantitative analyses of Figures 2G and 2H (see the revised Figures 2H and 2J), and statistical details are provided in the revised figure legends.

> *(3) Bar plots with standard error are not suitable for visualizing the distribution of data. Either show violin plots, histograms, or raw data points throughout.*

As suggested, we included the raw data points in the revised manuscript.

> *(4) Figure 3 legend - (Wen et al., 2010) citations repeated.*

Thank you for the comment. We have removed the repeated (Wen et al., 2010) citation in the revised manuscript.

> *(5) Does Ebbr4 deletion change the waveform shape of PV+ cells? This could influence spike sorting and cell classification.*

Thank you for the comment. According to your recommendations, we performed additional *ex vivo* patch-clamp recordings of PV+ interneurons, which showed that ErbB4 knockout did not alter their action potential waveform shape (e.g. spike amplitude and half-width, the revised Figure 7—figures supplement 1D and 1E). Importantly, this knockout also did not directly affect the spike waveform shapes of M/TCs *in vivo* (e.g. peak-to-valley ratio and half-valley width, the revised Figure 4—figures supplement 1C-1E). Therefore, we speculate that spike sorting and cell classification were not affected.

> *(6) Line 327 - is this really a measure of inhibitory circuit plasticity?*

Thank you for the comment. We have replaced "inhibitory circuit plasticity" with "inhibitory circuit activity" and comprehensively updated all relevant instances throughout the manuscript to ensure consistent use of the term.

> *(7) In the discussion: "Another interesting finding is that the changes in spontaneous firing rate differed for odor-evoked excitatory and inhibitory responses in vivo, suggesting that ErbB4 in PV interneurons dynamically regulates the spontaneous activity of M/TCs in response to different odors." The significance of this finding is not discussed and it is not clear what this result means. For example, does this relate to a "winner-take-all scenario"?*

Thank you for the comment. According to your recommendations, we have discussed the significance of this finding in the revised Discussion section (Lines 438-449):

This result reveals a dual regulatory role of ErbB4 in PV interneurons in olfactory coding. For odour-evoked excitatory responses, PV interneurons (via ErbB4) constrain M/TC spontaneous firing at a low baseline, minimising background noise and enhancing the SNR. In contrast, the inhibitory responses maintain a higher spontaneous firing baseline to accentuate odour-evoked suppression. This regulation amplifies the "excitation of excited M/TCs and inhibition of inhibited M/TCs," a hallmark of the OB's "winner-take-all" mechanism that sharpens odour identity coding, which is critical for odour discrimination. These data confirm that ErbB4 in PV interneurons does not exert a global modulation, but dynamically tailors M/TC spontaneous activity to odour-evoked responses, thereby optimising the ability of the OB to resolve olfactory cues.

> *(8) The discussion on linking AD with odor discrimination impairments, and the potential role of Erbb4 was interesting. However the discussion of "fluctuation status" is not defined. What does this refer to?*

According to the comment, we have added the following wording to the Discussion section (Lines 478-497):

As referenced by Iemi et al. (2022), "fluctuation status" herein refers to the spontaneous, endogenous fluctuations in neural activity that occur in the brain prior to sensory stimulation (i.e. pre-stimulus) or in the absence of external sensory input. External cues do not drive this state but arise from intrinsic neural dynamics, and it is primarily characterised by changes in the power of neural oscillations across multiple frequency bands (e.g., alpha, beta, and their neighbouring frequencies, collectively termed "alpha+ band" in Iemi et al. (2022)). Critically, this fluctuation status is distinct from stimulus-evoked neural responses; it reflects a pre-existing "baseline" state of the neural system that modulates subsequent sensory processing and behaviour. Consistent with Iemi et al. (2022), previous work has established that such ongoing neural fluctuations strongly predict behavioural variability in both health (e.g. slower reaction times and reduced perceptual accuracy) and disease (e.g. age-related cognitive decline and schizophrenia) by regulating neuronal excitability. In our study, we extended this concept to olfactory function, focusing on "broad ongoing fluctuations" (encompassing multiple frequency bands) and linking their dynamics to OB output. Specifically, these fluctuations influence the ability of the OB to support rapid recovery from olfactory adaptation and to mediate complex odour discrimination, thereby uncovering a novel role for endogenous neural fluctuation status in olfactory circuit function.

> ***Reviewer #3 (Recommendations for the authors):***
>
> *(1) For Figure 1C, I strongly recommend that the authors include full, uncropped Western blot images for both p-ErbB4 and total ErbB4 as supplementary material to improve the transparency and credibility of the findings.*

As you suggested, we have supplemented the full, uncropped western blot images for both phosphorylated ErbB4 (p-ErbB4) and total ErbB4, as the revised Figures 1 and 2 and Supplementary Figure 1.

> *(2) The authors should either validate the specificity of the sc-283 antibody in their experimental conditions or consider using a more specific antibody for ErbB4 to ensure the reliability of their data.*

Thank you for your comments. As shown in the revised Figure 2I and 2J, the absence of ErbB4 expression in PV-ErbB4 knock-out mice proved the specificity of the antibody for immunofluorescence staining. To address these potential concerns, we conducted a rigorous validation tailored to our model. In the revised manuscript, we complemented the protein-level detection with RT-PCR, which directly validated the specific knockout of *Erbb4* mRNA in PV neurones (the revised Figure 2F-H). Additionally, we performed follow-up immunofluorescence staining experiments using a well-validated anti-ErbB4 antibody (19943-1-AP, Proteintech; see PMID: 37060105) to assess the expression of ErbB4 in PV neurones (the revised Figure 9B and 9C).

> *(3) I recommend that the authors clarify in the methods section whether a post hoc test with multiple comparison adjustments (e.g., Tukey's HSD or Bonferroni) was conducted for the behavioral tests presented throughout the study. If no such test was performed, it would be beneficial to include one to ensure accurate identification of significant differences between groups across the different experimental days or conditions.*

For the behavioural tests, we confirmed that two-way ANOVA was followed by Tukey's post hoc adjustment for multiple pairwise comparisons, which has been clarified in the revised Methods section (Lines 832-833). Additionally, we have revised the asterisks in the relevant figures to clearly indicate significant post-hoc differences between the groups.

> *(4) The rationale for using a whole-brain PV-specific knockout model (PV-ErbB4-/-) to assess OB-specific phenomena in Figures 4 and 5 should be clarified. I also recommend the authors provide or conduct additional experiments with OB-specific knockouts to determine whether the effects observed in Figures 4 and 5 are directly attributable to the loss of ErbB4 in PV interneurons within the OB.*

To clarify the rationale, the whole-brain PV-*Erbb4*$^{-/-}$ mouse line was initially used to characterise the overall functional relevance of ErbB4 in PV interneurons for OB activity and odour-evoked responses. We clarified this rationale in the revised Results section (Lines 210-211 and Lines 250-251).

As elaborated above, AAV-mediated OB-specific knockouts suffer from injection-induced tissue injury, incomplete mosaic recombination, and uncertainties in local electrophysiological recordings, which would compromise data reliability. Moreover, OB PV interneurons act predominantly as local circuit neurones; therefore, the phenotypes observed in Figures 4 and 5 most plausibly arise from intrinsic ErbB4 deletion within bulbar PV cells rather than from long-range brain-wide network changes. For these reasons, we consider our current global PV-*Erbb4*$^{-/-}$ model appropriate to interpret the local OB circuit effects here, and we outline OB-targeted knockout manipulations as a direction for future independent follow-up research.

> *(5) To strengthen their conclusions drawn from Figures 6-8, the authors should perform direct recordings from PV interneurons in the OB to assess how the ErbB4 knockout affects their intrinsic properties, synaptic inputs, and firing behavior. This would provide more direct evidence of PV interneuron dysfunction in the knockout mice.*

According to your recommendations, we have performed direct recordings of OB PV interneurons using *ex vivo* patch-clamp electrophysiology (the revised Figure 7—figures supplementary 1). These recordings reveal that ErbB4 knockout affects the intrinsic properties of PV interneurons, synaptic inputs (reduced mEPSC frequency and amplitude, the revised Figure 7—figures supplementary 1A and 1B), and firing behaviour (increased action potential frequency, the revised Figure 7—figures supplementary 1C), directly confirming that ErbB4 deletion affects PV interneurons themselves. These results provide direct evidence of PV interneuron dysfunction in the knockout mice.

> *(6) I recommend that the authors assess molecular markers of PV interneuron inhibition, such as GAD67, in PVIs. This would help link the ErbB4 knockout to impaired PV interneuron function and its downstream effects on MC inhibition.*

Thank you for the comment. We attempted to detect GAD67 in OB PVIs using multiple commercial antibodies but encountered consistent technical limitations (e.g. weak signal specificity and high background) that precluded reliable quantitative analysis.

To address this gap, we used optogenetics to activate PV interneurons and recorded optogenetically evoked inhibitory postsynaptic currents (oIPSCs) in MCs. As shown in the revised Figure 9 and Supplementary Figure 1F and 1G, deleting ErbB4 of PV interneurons in the OB weakened the inhibitory modulation of MCs by PV interneurons. This result provides direct electrophysiological evidence linking ErbB4 knockout to impaired PV interneuronal function and its downstream effects on MC inhibition.

> *(7) For Figure 9, I recommend that the authors perform IHC to show that ErbB4 is selectively knocked out in PV neurons but not in non-PV neurons within the OB, as the Western blot analysis alone does not provide this specificity.*

According to your recommendations, we performed an additional key experiment: immunofluorescence co-staining for PV and ErbB4, with quantitative analysis confirming a significant reduction in ErbB4 in OB PV interneurons, but not in non-PV cells, in AAV-PV-Cre–injected mice (the revised Figure 9B and 9C).

https://doi.org/10.7554/eLife.101237.2.sa0